**Czech University of Life Sciences Prague**
**Faculty of Environmental Sciences**

**Department of Water Resources and Environmental Modelling**
**Study Program: Nature Conservation**

# Master's Thesis

# Geomorphological Variations of Northern Terra Cimmeria Watersheds

**Author:** Ghada Sultan
**Supervisor:** doc. Mgr. Ing. Ioannis Markonis, Ph.D
**Year:** 2023

# CZECH UNIVERSITY OF LIFE SCIENCES PRAGUE

Faculty of Environmental Sciences

# DIPLOMA THESIS ASSIGNMENT

BSc. Ghada Sultan

Nature Conservation

Thesis title

**Geomorphological Variations of Northern Terra Cimmeria Watersheds**

---

**Objectives of thesis**

The main objective of this thesis is to comprehensively identify and analyze geological landforms on Mars and investigate their relationship with potential water and movement on the planet's surface. The study will focus on the southern hemisphere of Mars for a Late-Noachian period. Specifically, we aim to search for structures such as paleolakes, craters, alluvial fans, and pingos and determine if they are connected to a valley network. We will identify the landforms to explain their unique structures and characteristics. This study is expected to provide significant contributions to our understanding of the geology of Mars and its potential for harboring water and supporting movement.

**Methodology**

A new Martian valley network/basin dataset is currently being derived from CTX imagery. It opens a new way to quantify the processes which shaped these valley networks by linking the specifics of the intra sub-basins geomorphology (reoccurring landforms). With this approach we can link the "juiciest" and "driest" areas of Terra Cimmeria to specific geographical settings and geomorphological features and shed light of the fluvial, glacial and lacustrine development of the area. Review part will be focused on overview of geomorphological evidence of the valley fluvial, glacial and periglacial activity (polygonal ground patterns, pingos, lakes, etc.). Practical part will consist of geomorphological mapping/search for shapes described in the review part. This is done using CTX mosaic data to explore geological landforms that are potentially related to water. Then, delineate landforms using ArcGIS, and calculate geomorphometry data and elevation within the landforms using MOLA-DEM data. Finally, describe and compare the obtained data with existing literature.

**The proposed extent of the thesis**

**Keywords**

Mars geomorphology, Late-Noachian, Water related landforms, Paleolakes, Alluvial fans

---

**Recommended information sources**


Caleb I. Fassett, & James W. Head III. (2008). Valley network-fed, open-basin lakes on Mars: Distribution and implications for Noachian surface and subsurface hydrology. In Icarus (Vol. 198, Issue 1, pp. 37–56). American Geophysical Union. https://doi.org/10.1029/2004JE002287

Carr, M. H., & Head, J. W. (2010). Geologic history of Mars. Earth and Planetary Science Letters, 294(3–4), 185–203. https://doi.org/10.1016/j.epsl.2009.06.042

Carr, M. H., & Head, J. W. (2015). Martian surface/near-surface water inventory: Sources, sinks, and changes with time. Geophysical Research Letters, 42(3), 726–732. https://doi.org/10.1002/2014GL062464

Goudge, T. A., Aureli, K. L., Head, J. W., Fassett, C. I., & Mustard, J. F. (2015). Classification and analysis of candidate impact crater-hosted closed-basin lakes on Mars. Icarus, 260, 346–367. https://doi.org/10.1016/j.icarus.2015.07.026

Tanaka, K. L., Skinner Jr, J. A., Dohm, J. M., Irwin III, R. P., Kolb, E. J., Fortezzo, C. M., ... & Hare, T. M. (2014). Geologic map of Mars.

Vijayan, S., & Mangold, N. (2021). Evidence for fluvial and glacial activities within impact craters that excavated into a Noachian volcanic dome on Mars. Icarus, 361, 114397.


---

**Expected date of thesis defence**

2022/23 SS – FES

**The Diploma Thesis Supervisor**

doc. Mgr. Ing. Ioannis Markonis, Ph.D.

**Supervising department**

Department of Water Resources and Environmental Modeling

Electronic approval: 30. 3. 2023

**prof. Ing. Martin Hanel, Ph.D.**

Head of department

Electronic approval: 30. 3. 2023

**prof. RNDr. Vladimír Bejček, CSc.**

Dean

Prague on 30. 03. 2023

**Author's Statement**

I hereby declare that I have independently elaborated the diploma/final thesis with the topic of: Geomorphological Variations of Northern Terra Cimmeria Watersheds and that I have cited all the information sources that I used in the thesis and that are also listed at the end of the thesis in the list of used information sources. I am aware that my diploma/final thesis is subject to Act No. 121/2000 Coll., on copyright, on rights related to copyright and on amendment of some acts, as amended by later regulations, particularly the provisions of Section 35(3) of the act on the use of the thesis. With my own signature, I also declare that the electronic version is identical to the printed version.

In Prague on 31st March 2023 Ghada Sultan

**Acknowledgement**

I am grateful to acknowledge the invaluable support and guidance provided by my supervisor, doc. Mgr. Ing. Ioannis Markonis, Ph.D. I would also like to extend my sincere appreciation to my advisor, MSc. Cuřín Vojtěch, for his indefinite support and assistance.

Ghada Sultan

*Thesis Title:*

**Geomorphological Variations of Northern Terra Cimmeria Watersheds**


| | |
|---|---|
| *Author:* | Ghada Sultan |
| *Study Field:* | Nature Conservation |
| *Study Program:* | Environmental Modelling |
| *Type of thesis:* | Master Thesis |
| *Supervisor:* | doc. Mgr. Ing. Ioannis Markonis, Ph.D |
| | Department of Water Resources and Environmental Modelling |
| *Consultant* | MSc. Cuřín Vojtěch |
| | Department of Water Resources and Environmental Modelling |

*Abstract:* Mars' geomorphology offers a valuable insight into the planet's physical and geological characteristics, including its potential for water presence and distribution across its surface. High-resolution satellite images have revolutionized the study of Martian geomorphology, enabling scientists to investigate the planet's surface features in detail and with greater efficiency. This offers a unique opportunity for understanding the processes that shape planetary surfaces, particularly the role of water in shaping landscapes. This study aims to investigate the geomorphological characteristics of the surface of Mars in the southern hemisphere near the equator, and how these characteristics provide insight into the planet's water forms and quantities. High-resolution satellite images were utilized to efficiently analyze the landforms related to water flow and formulation in the study area, which spans from 133.228 to 127.9 Longitude and -5.439 to -11.096 Latitude. By applying morphometric analysis to the landforms' area, elevation, and volume, we were able to compare the characteristics of the landforms to those found on Earth and to previously detected landforms on Mars. The results revealed the presence of alluvial fans, open-basin and closed-basin lakes, craters, and other forms that can be connected to the valley system in the area of interest. One identified alluvial fan displayed similar geomorphological characteristics to those found on Earth and Mars, and the slope suggested the presence of gravel sediments. Additionally, the study identified a total of 7 open-basin lakes and 2 closed-basin lakes within the study area, which were formed during the Late-Noachian era. Furthermore, 11 craters were identified, with 3 of them displaying fans and ridges structures, indicating the flow of water within them. The identification of these features suggests that water has played a role in shaping the Martian landscape, particularly in the study area. The results provide overview into the geomorphology of Mars and its potential for water presence, which is crucial for Mars exploration missions. Further investigation of Mars' surface and the role of water in shaping its landscape is important particularly in the search for signs of past or present water on the planet.

*Key words:* Mars geomorphology, Late-Noachian, Water related landforms, Paleolakes, Alluvial fans.

*Název práce:*

**Geomorfologické rozdíly povodí Severní Terra Cimmeria**


| | |
|---|---|
| *Autor:* | Ghada Sultan |
| *Studijní obor:* | Ochrana přírody |
| *Studijní program:* | Environmentální modelování |
| *Typ práce:* | Diplomová práce |
| *Vedoucí:* | doc. Mgr. Ing. Ioannis Markonis, Ph.D |
| | Katedra vodních zdrojů a environmentálního modelování |
| *Konzultant:* | MSc. Cuřín Vojtěch |
| | Katedra vodních zdrojů a environmentálního modelování |



*Abstrakt:* Geomorfologie Marsu nabízí cenné poznání o fyzikálních a geologických vlastnostech planety, včetně jejího potenciálu pro výskyt vody a její distribuci na povrchu. Vysokorozlišovací satelitní snímky revolučně změnily studium geomorfologie Marsu, umožňujíce vědcům podrobněji a efektivněji zkoumat povrchové rysy planety. To nabízí jedinečnou příležitost porozumět procesům, které utvářejí povrchy planet, zejména úloze vody při tvarování krajiny. Tato studie si klade za cíl zkoumat geomorfologické vlastnosti povrchu Marsu v jižní hemisféře poblíž rovníku a jak tyto vlastnosti poskytují informace o vodních formách a množstvích na planetě. Vysokorozlišovací satelitní snímky byly využity k efektivní a přesné analýze pozemních tvarů souvisejících s prouděním a tvorbou vody v oblasti studie, která se rozprostírá od zeměpisné délky 133,228 do 127,9 a zeměpisné šířky -5,439 do -11,096. Použitím morfometrické analýzy oblasti pozemních tvarů týkajících se plochy, nadmořské výšky a objemu jsme byli schopni porovnat vlastnosti pozemních tvarů s těmi nalezenými na Zemi a s předtím objevenými pozemními tvary na Marsu. Výsledky odhalily přítomnost aluviálních kuželů, otevřených a uzavřených jezer, kráterů a dalších forem, které lze spojit s údolním systémem v oblasti zájmu. Jedno z identifikovaných aluviálních kuželů ukázalo podobné geomorfologické vlastnosti jako ty nalezené na Zemi a Marsu a sklon naznačoval přítomnost štěrkových sedimentů. Kromě toho bylo v oblasti studie identifikováno celkem 7 otevřených jezer a 2 uzavřená jezera, která vznikla v době pozdního noachiánu. Dále bylo identifikováno 11 kráterů, z nichž 3 zobrazovaly kuželovité a hřebenovité struktury, což naznačovalo proudění vody uvnitř nich. Identifikace těchto rysů naznačuje, že voda hrála roli při tvarování marsi.



*Klíčová slova:* Marská geomorfologie, Pozdní Noachian, Vodou související tvary terénu, Paleojezera, Říční kužely.

# Table of Content

# 1 Introduction

The history of Mars is a complex and geologists have identified several distinct eras that help us understand the evolution of the planet over time. These eras are defined based on the geographical and climatic conditions that are thought to have existed on Mars at different points in its history (Tanaka et al., 2014a). The presence of water on Mars is also known to have varied throughout the planet's history, with some periods being more conducive to the presence of liquid water than others (Carr & Head, 2015). For example, during the Noachian era, it is believed that Mars had a denser atmosphere and warmer climate, which may have allowed liquid water to exist on the planet's surface. In contrast, during the Amazonian era, Mars is believed to have had a much colder and drier climate, with much less water present on the planet's surface (Lammer et al., 2005).

The exploration of Mars has revealed the presence of various forms of water on the planet, including ice, liquid water, and groundwater. The Martian polar caps contain water ice, and recent studies have suggested that there could be vast underground reservoirs of ice on the planet (Head et al., 2003). The detection of networks of valleys in satellite images is also suggestive of the past presence of liquid water on the planet's surface. These valleys are believed to have formed due to the erosion caused by the flow of water over extended periods of time (Rosenberg et al., 2019).

The study of the volume of water on Mars is a crucial aspect in understanding the planet's geological and climatic history. Previous estimates of the amount of water on the planet have been controversial, with varying estimates from a few meters of GEL[1] to the possibility of oceans existing in the past (Carr & Head, 2015). Recent advancements in technology and data collection have allowed for more accurate measurements of the amount of water-ice present at the near-surface of Mars. These improved measurements have led to a better understanding of the water budget on the planet and its potential to participate in geologic processes. Recent studies have revealed a diverse range of water-related landforms that suggest the presence of liquid water on Mars in the past Conway & Balme, 2014). Among these landforms are valley networks, open-basin lakes, closed-basin lakes, channels, fluvial terraces, and deltas. Each of these landforms has unique geomorphological characteristics that can be observed using high-resolution satellite images. These images allow scientists to distinguish these landforms from one another and to better understand the Geomorphology of Mars. By

[1] Global Equivalent Layer

studying the metrological data of these landforms, their relation to the water is assessed. This helps us to understand how we can contribute to the flow of water and how the water can formulate the structure of these landforms. The identification of these water-related landforms is crucial in understanding the planet's hydrological system and its potential to host life in the past or present.

In order to better understand the water inventory on Mars, landforms, and their applicability to hold water in the past through studying the evidence of various landforms on Mars, such as alluvial fans, open-basin and closed-basin lakes and channels, finding out the role of these landforms in the construction of the area and their role as water inventory and providing more insights into the geographical record of Mars and the potential for the existence of life in the past or in the future.

# 2 Objectives and Methodology

## 2.1 Objectives

The main objective of this thesis is to comprehensively identify and analyze geological landforms on Mars and investigate their relationship with potential water and movement on the planet's surface. To accomplish this, we will utilize high-resolution CTX[2] stereo and CTX mosaic images to delineate landform structures and employ the ArcGIS software as a tool for image visualization and conducting geomorphological analysis. The study will focus on the southern hemisphere of Mars, covering an area of 46,957.8 square kilometers for a Late-Noachian period. Specifically, we aim to search for structures such as paleolakes, craters, alluvial fans, and pingos and determine if they are connected to a valley network. We will meticulously and accurately identify the landforms to explain their unique structures and characteristics. Furthermore, we will conduct a comparison with terrestrial and martial literature to validate the findings. This study is expected to provide significant contributions to our understanding of the geology of Mars and its potential for harboring water and supporting movement**.**

## 2.2 Methodology

- Utilize CTX mosaic data to explore geological landforms on Mars that are potentially related to water.
- Visualize the Martian surface using ArcMap in ArcGIS to gain insights into the geology of the planet.
- Delineate landforms using edit session and create feature functions in ArcGIS, ensuring accuracy in the process.
- Calculate elevation within the landforms using MOLA-DEM[3] data, enabling a more comprehensive understanding of the geology.
- Employ basic functions from ArcToolbox to calculate Geomorphometric data, such as area, slopes, and aspects, which can provide further insights into the features and characteristics of the landforms.
- Analyse and process obtained data, ensuring that statistical techniques and scientific methods are employed.
- Describe and compare the obtained data with existing literature to validate the results and provide a broader context for the findings.

[2] Context Camera
[3] The Mars Orbiter Laser Altimeter - Digital Elevation Model

# 3 Literature Review

## 3.1 Mars Water Inventory

Quantifying the water inventory on Mars is crucial for understanding the availability and distribution of water on the planet. This includes the presence of liquid, vapour, and Ice water. Different methods may be used to measure the water inventory depending on the form and location of the water. The available amount of water that participates in geologic processes at or near the surface of Mars is not certain (Carr & Head, 2015). The presence of water on Mars is indicated by the Global Equivalent Layer (GEL), which refers to the depth of water if it were evenly distributed across the planet, rather than being trapped in valleys or underground networks. One of the suggested theories is that there were oceans in the Hesperian and Amazonian era covering the northern plains of Mars, which in turn supports the existence of GEL in the liquid form, estimated to be hundreds of meters to kilometres (Baker et al., 1991). This is opposite to the previous conclusion that the GEL only held few meters (Yung et al., 1988).

### 3.1.1 Ice

Mars is known to contain significant amounts of ice, both in its polar regions and in other areas such as mid-latitudes landforms, and underground in the subsurface (Head et al., 2003). The majority of ice on Mars is found in the polar regions, which are covered by extensive ice sheets that can reach thousands of meters in thickness. It has several types of ice deposits, including seasonal deposits of CO2 ice in the polar regions, residual ice caps consisting of water ice, and Polar Layered Deposits (PLD) consisting of layers of ice mixed with dust. The seasonal deposits of CO2 ice formed from the condensation of the atmosphere and lasting through the Martian winter, with a thickness of less than one meter while the residual ice caps partially cover the polar ice sheets and are made up of high-albedo water ice deposits with a thickness much less than the ice sheets themselves (Head et al., 2003). Underneath them are the PLD, consisting of hundreds of layers of water ice and dust with varying proportions based on the climatic conditions at the time of deposition. The total volume of ice currently present on Mars is estimated to be equivalent to a 34 GEL with 22 meters of that in the polar water ice cap (Plaut et al., 2007).

Ice on Mars can also be found in the latitude-dependent mantle (LDM) Layer. LDM is a morphological unit that covers a significant portion of Mars' surface outside of the polar regions. It is thought to contain the bulk of the planet's shallow ground ice.

The LDM has been linked to observations of present-day, massive ground ice in the upper tens of centimeters of Mars' surface by remote sensing and by identification of high albedo, swiftly fading deposits within newly formed impact craters at mid-latitudes (Schon et al., 2012). The LDM is interpreted to be a mixture of ice and dust based on the presence of thermal contraction polygons and sublimation-like degradation pits. It is estimated to be young (0.1-1 Ma) and in places comprises at least six layers. On cold pole-facing slopes in the mid-latitudes, the LDM often blankets the middle and lower parts of the slope, infilling local hollows, and has a well-defined, lobate margin near the top of the slope. Erosional gullies occur in such LDM deposits, inspiring suggestions that it is analogous to a "pasted-on" snowpack (Figure 3.1). The LDM in such regions exhibits polygonal patterns associated with thermal contraction, crevasse-like fractures, downslope lineations, and steep gully incisions (Conway & Balme, 2014). This "pasted-on" LDM overlies other putatively ice-rich deposits, such as concentric crater fill (Figure 3.2). The volume of the source alcoves and terminal deposits of gullies can be used to investigate the composition of the LDM.

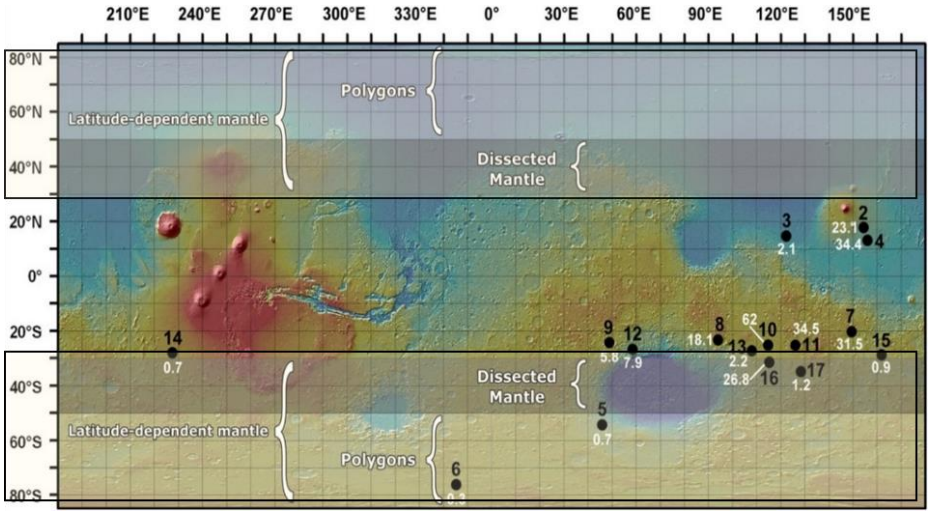


**Figure 3.1:** Layers of ice-rich latitude-dependent mantling (LDM) found in the northern and southern martial hemispheres (Schon et al., 2012).

Different hypotheses are suggested to explain the formation of ice in the LDM. The main hypotheses are that the ice formed through slow vapor diffusion of water vapor into the regolith, or through direct emplacement of ice as snow or frost accumulation, or frozen liquid water (Fisher, 2005). Moreover, ground ice stability in the mid-latitudes of Mars is influenced by the planet's orbit and axial tilt. There are a variety of landforms in the mid-latitudes that resemble ice-rich landscapes on Earth, but their creation cannot be attributed to periodic changes in the climate. Some of the geomorphic landforms in the region are believed to have formed from the viscous flow of ice-rich materials, including lobate debris aprons (LDA), lineated valley fill (LVF),

and concentric crater fill (CCF). These features can be tens of kilometers in size and are thought to be from the Early to Middle Amazonian period (Berman et al., 2021).

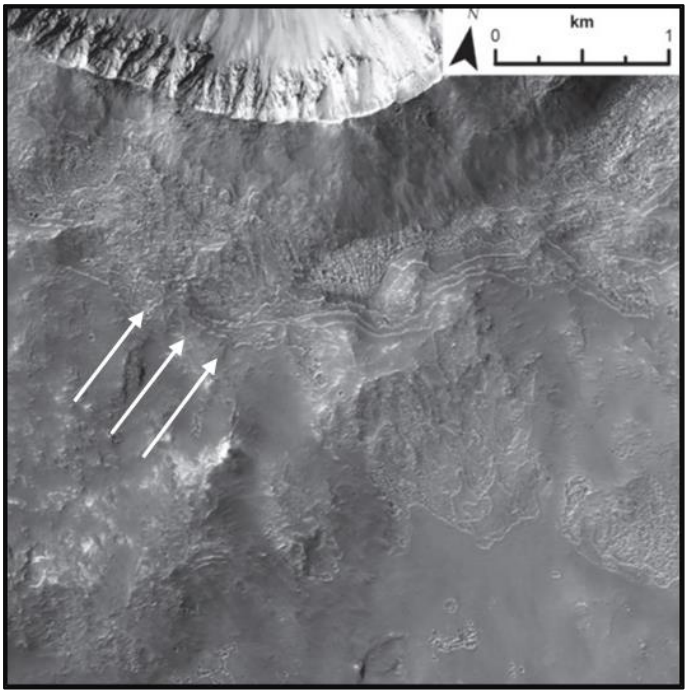


**Figure 3.2:** Geomorphic evidence of multiple layers of remnant LDM latitude dependent mantling in a crater in Terra Sabaea (Schon et al., 2012).

### 3.1.2 Liquid Water

The total volume of liquid water present on early Mars has also been estimated through various methods, such as the study of geological features believed to have been carved by water. An example of these studies was shown by (Rosenberg & Head, 2015) where the amount of water needed to shape the valley networks was intially estimated by utilized the valley network distribution information (Williams & Phillips, 2001) and the volumes of eight major valley networks (Hoke et al., 2011) gathered to determine the volume of sediment removed during the carving of the networks. This was based on the Mars Orbiter Laser Altimeter (MOLA) data with a resolution of 460 m/pixel. Then, a fluid-to-sediment flux ratio used to estimate the minimum amount of water required and the total amount of sediment removed from the networks. The result was an estimate of 3-100 m for the required volume of water in the form of GEL (Rosenberg et al., 2019).

The ratio between normal and deuterated water on Mars has also changed over time, with lighter $H_2O$ molecules escaping the planet more easily than heavier heavy water (HDO), which confirms the loss of a large quantity of water over time. It has been estimated that the total water present on the surface of Mars 4.5 billion years ago was 6-7 times the current amount (Villanueva et al., 2017).

Liquid water is thought to have once flowed on the surface of Mars, but today it can only be present briefly and under uncommon circumstances due to the planet's low temperature and atmospheric pressure. The discovery of networks of narrow, incised channels called gullies on Mars, which are thought to have been carved by groundwater seepage and surface runoff, provided the first evidence of a recent occurrence of liquid water on the planet's surface (Orosei et al., 2020). The formation of gullies has been explained through different mechanisms, with liquid-water debris flows resulting from surface melting being considered the most plausible (Figure 3.3). The mapping of gullies on the Martian surface has shown that they occur in specific latitude bands and that their presence is anti-correlated with massive ice deposits (Jouannic et al., 2012). They are considered to be among the most promising locations for evidence of past or present liquid water on the planet (Dundas et al., 2010). Recent studies have provided evidence for subglacial liquid water beneath the South polar cap through orbital radar sounding, but the exact amount and location of this water is still being studied and debated (Orosei et al., 2018, 2020b). Understanding the presence and distribution of liquid water on Mars is crucial to explore the geology of the planet.

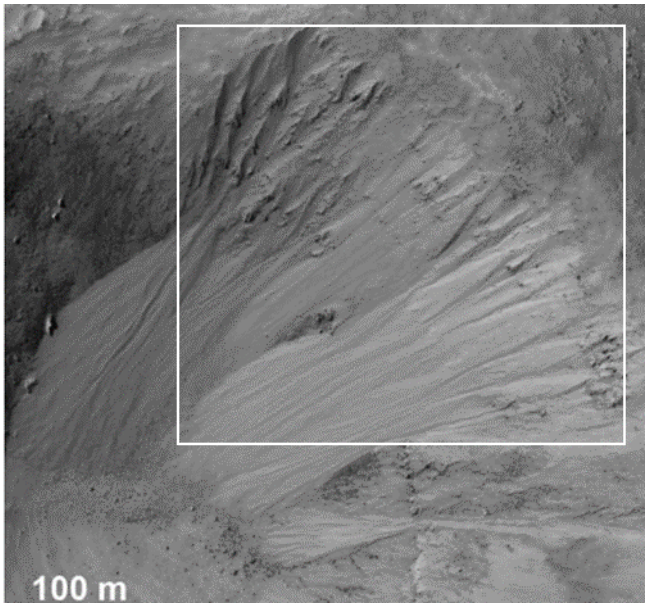


**Figure 3.3:** Gully like-landform suggested to be formed by melted ice (Dundas et al., 2019).

Studies have suggested that the gullies on Mars may have formed as a result of the melting of subsurface ice during warm periods, or as a result of liquid water seeping out of underground aquifers and flowing down the slopes of craters and valleys (Conway et al., 2018). Some studies have also suggested that the formation of gullies may be related to climatic changes on the planet, and that they may have formed as a result of the periodic melting of polar ice caps or of the of the Martian ice-rich deposits LDM . The occurrence of Martian gullies is correlated with the distribution of water ice landforms. Gullies are found in the same latitudes as various range of ice related

landforms but are less common in areas with high concentrations of LDA, and they are only seen in 12% of craters with interior ice deposits (Conway et al., 2018).

### 3.1.3 Groundwater

The hydrologically underdeveloped landscape of early Mars likely played a significant role in shaping the watershed of valley networks. The limited availability of liquid water on the surface of Mars likely prevented the evolution of extensive river systems and instead favored the development of groundwater systems. The groundwater on early Mars likely flowed through the subsurface and contributed to the formation and evolution of valley networks. Prior to the Amazonian and Hesperian periods, the water suggested to infiltrate the surface and move through the crust and recharge the groundwater system (Caleb I. Fassett & James W. Head III, 2008). This is supported by the presence of hydrological features, such as fan-shaped deposits, on the floor of many valleys, which are interpreted as evidence of groundwater discharge (Caleb I. Fassett & James W. Head III, 2008).

For surface water, watersheds are areas separated by a topographic divide line with identified highest points on the land surface. However, this definition may not be effective in studying groundwater, as the divide between basins can differ from the topographic divide and result in inter-basin groundwater flow (IGF) (Winter et al., 2003). The exact description of groundwater divides is necessary to understand the features of IGF. Traditionally, groundwater divide explained as a curve on the water table ridge, which separates the flow domain into subdomains (Winter et al., 2003). The relationship between the groundwater divides and the top of the water table in a river basin explained in Figure 3.4. They found that a pass-through flow may develop below the local flow systems when the groundwater is close to the high river (Han et al., 2019).

Moreover, the underground water could influence the watershed of valleys by affecting the distribution of sediment, influencing the incision of valleys, and contributing to the creation of specific landforms, such as alluvial fans, craters and lakes, that are associated with groundwater discharge. The interplay between the subsurface water and the surface landscape likely played a crucial role in shaping the watershed of valley networks on early Mars (Caleb I. Fassett & James W. Head III, 2008).

To add, the presence of groundwater depends on the heat flow, with groundwater lasting only at latitudes exceeding 30° for chondritic heat flow (Grimm & Painter, 2009). The presence of gullies in certain latitudes and on nonequatorial slopes suggests that the gradual percolation of groundwater to the surface and its evaporation must be impeded by an ice barrier, which allows for the formation of a reservoir of liquid. The

eventual outburst of this ephemeral reservoir transports accumulated debris downslope as a slurry flow of ice, liquid, and rock debris. The eventual outburst of this ephemeral reservoir transports accumulated debris downslope as a slurry flow of ice, liquid, and rock debris. In amodel explains why gullies are not found in regions with higher temperatures and equator-facing slopes, suggesting that emergent groundwater would quickly evaporate, preventing the persistence necessary for gully formation (M. C. Malin & Edgett, 2000). The model involves groundwater moving within and along bedrock layers, until it reaches the surface and creates a depression (M. C. Malin & Edgett, 2000).

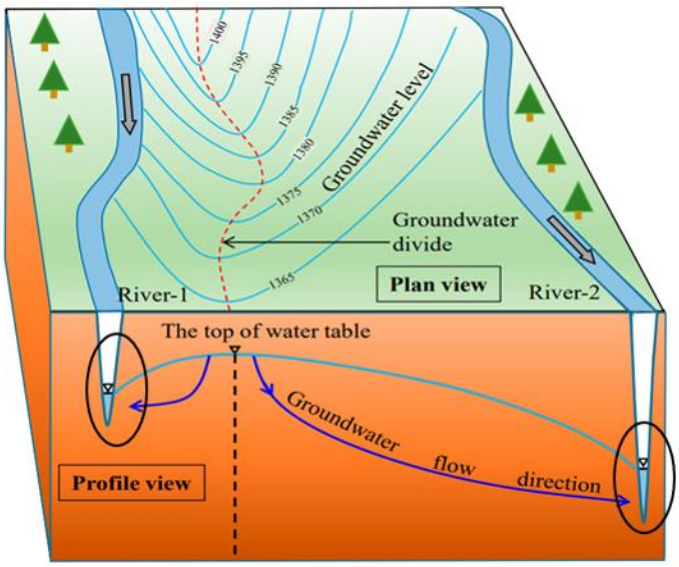


**Figure 3.4:** A Model explains the divides of groundwater in case of two valleys that have two different water tables (Han et al., 2019).

### 3.1.4 Outflow Channels Formation

The presence of ancient fluvial features on the surface of Mars, including valley networks, open-basin lakes, and closed-basin lakes, indicate the presence of liquid water and related fluvial and lacustrine processes on the surface of the southern highlands during the Late Noachian period (Caleb I. Fassett & James W. Head III, 2008). These features are usually taken to imply a "warm and wet" climate with rainfall and the potential for oceans in the northern lowlands. It is suggested that liquid water was not stable on the surface of Mars during the Late Noachian period, but transient liquid water (melted ice) may have occurred if surface temperatures were between the melting and boiling points (Richardson & Mischna, 2005). It has been found that at higher obliquities and slightly higher surface pressures, conditions suitable for transient liquid water are met over a large area of Mars. However, as surface pressure increases, atmospheric thermal blanketing reduces the diurnal temperature range, making it impossible for transient liquid water to occur. On the other hand, at high enough pressures, the mean annual temperature is sufficient to allow stable liquid water (Richardson & Mischna, 2005). One conclusion from these studies is that the potential for liquid water

on Mars has not decreased monotonically over time as the atmosphere was lost, but rather, there was a minimum in the potential for transient liquid water during a period with pressures in the range of 0.1 to 1 bar. It indicates similar conditions to those that may have existed in the Noachian, predict a "warm and wet" climate, characterized by continuous conditions suitable for the stability of liquid water on the surface (Palumbo et al., 2018).

The formation of outflow channels on Mars, are believed to have been formed by the eruption of groundwater from beneath a thick layer of ice. Floods may be limited in their ability to erode and shape the landscape not by their power, but by their ability to carry sediment. In approximate, a total of 40 meters of water were required to form the large circum-Chryse channels, based on assumptions about the sediment load carried by large floods and 20% by volume of the canyons (Carr & Head, 2015). The estimated volume of water brought to the surface in the development of outflow channels is highly uncertain due to the difficulty in distinguishing between tectonic and erosional processes in the formation of the channels. The largest outflow channel, Kasei Vallis, is estimated to have resulted from the erosion of 4.8 m GEL of water, while the large Chryse channels are estimated to have resulted from the erosion of approximately 10 m GEL of water (Carr & Head, 2015). However, it is possible that the actual volume of water involved could be higher or lower due to uncertainties in the sediment load and the proportion of tectonic versus erosional processes in the development of the channels.

## 3.2 History of water on Mars

### 3.2.1 Evidence for The Presence of Water on Mars

The evidence for water flow on Mars can be observed in different locations such as in Terra Cimmeria. The northern segment of the Sirenum Fossae in Terra Cimmeria contains two craters filled with smooth and concentric crater fill material, which is believed to be ice-rich based on its behavior and the behavior of similar material elsewhere on Mars. On the floor of the western fluvial system, there are several deposits with convex-upward profiles and crevasses on their surfaces that are believed to be ice-rich as well. These well-preserved ice-rich deposits suggest a prolonged glacial history in Terra Cimmeria during the early to middle Amazonian period (Adeli et al., 2016). The intermediate section does not show direct traces of fluvial activity, but it may have had a different morphology at the time of the fluvial activity and may have been a depression to collect surface runoff. The surface of the bedrock unit is locally polygonally fractured, which may indicate liquid water activity similar to a lacustrine environment. The mantling unit is more concentrated in the western and northern part of the intermediate section and corresponds to the middle Amazonian. This suggests that it may be a drape of frozen dust deposited during a middle

Amazonian ice age and revealing one or several recent Amazonian glacial history (Conway & Balme, 2014). The erosional and depositional features of the fluvial system in Terra Cimmeria, including incised channel floors, fan deltas, and alluvial fans, suggest highly energetic and short-term fluvial activity. Similar valleys and landforms of Amazonian age in other mid-latitude regions have been interpreted as being formed by a single, short fluvial episode (Adeli et al., 2016). Likely, the water source for the short-term event events is surface runoff of ice melt, which would have occurred under different climatic conditions in the past. They are triggered by obliquity or orbital variations that mobilized polar ice towards mid-latitude regions of Mars.

Another example of the presence of water On mars is the depression at the head of Karun Valles. This depression could have hosted an ice-covered lake or a subglacial lake, which collapsed and initiated a catastrophic outflow. The liquid water collected by the upstream catchment system may have fed the depression and formed an ice-covered lake under middle Amazonian atmospheric conditions. Alternatively, the depression may have hosted a glacial deposit, which catastrophically collapsed and melted. An alternative source of water could be rise of groundwater, but this would not explain the distribution of small depressions and ice-rich deposits on various locations and elevations (Hobley et al., 2014).

### 3.2.2 Geomorphological and Water History of Mars:

The history of Mars can be divided into several distinct eras, based on the geologic and climatic conditions that are thought to have existed on the planet over time. The earliest era is Noachian period estimated to be between 4.1 to 3.7 billion years ago, while Hesperian period is approximately from 3.7 to 3.0 billion years ago, and Amazonian period which started from 3.0 billion years ago to present (Carr & Head, 2010).

The Noachian Period on Mars was a time of intense geological activity, with significant modification of the Martian surface due to impacts, volcanic activity, and erosion (Carr & Head, 2010). The presence of isolated volcanic constructs, such as the Tharsis Montes and Elysium Mons, suggests that volcanic activity was not limited to the Noachian highlands and that volcanic activity was regionally and temporally varied during this time (Tanaka et al., 2014a). The modification of the cratered highlands on Mars continued into the Late Noachian period with processes such as volcanism, sedimentation, and impact events, although at a reduced rate and extent compared to earlier periods. The early Noachian highlands are thought to consist of less proportion of sedimentary and volcanic materials compared to Middle Noachian highlands (mNh), which may be a reflection of the climate conditions that were conducive to precipitation and runoff during the mNh (Tanaka et al., 2014a).

The Hesperian Period on Mars was characterized by extensive geological activity, including volcanism, tectonism, chaos, and outflow channel development (Carr & Head, 2010). The period also saw a decrease in the overall formation of precipitation-fed runoff valleys and sedimentary deposits, with most occurring in local highland areas. The period was dominated by acidic weathering conditions, leading to sulfate enrichment of layered deposits in Valles Marineris, Gale crater, and other highland craters (Tanaka et al., 2014a).

While in the Amazonian period, the environment on Mars was characterized as cold, dry, and oxidizing. Despite being the longest geologic period on Mars, the rates of material deposition and cumulative amounts of geologic modification were significantly reduced compared to previous epochs (Carr & Head, 2010). The Amazonian period was dominated by accumulation of polar layered deposits, dunes, and possible relict mountain glacial moraines. Magmatic-driven processes may have also contributed to environmental change during this period. The resulting geologic composition are complex (Tanaka et al., 2014a). They reflect a dynamic and changing environment, but also provide a window into the history of Mars.

### 3.2.3 Water Content and Movement Through History

The climate and hydrological regime in the Late Noachian period of Mars' history was characterized by repetitive episodes of precipitation and surface runoff, as opposed to the mainly episodic groundwater eruptions that occurred later (Carr & Head, 2010). Higher rates of geothermal heat flux, impact rates, crater degradation, volcanism, and aqueous alteration to form clays may have allowed more water to infiltrate into the ground or be chemically fixed in the subsurface. The near-surface inventory of water during this period is estimated to be 24 m GEL, but the total amount of water presents at the surface and within the upper few kilometers of Mars’s surface is thought to be higher, possibly including 120 m GEL of water outgassed during the formation of Tharsis (Lammer et al., 2005). The absence of oceans at this time and the low near-surface water inventory supports a model of a cold, icy climate with water concentrated in ice sheets. The current surface and near-surface water budget of 34 m GEL could have formed valley networks through repeated episodes of melting and runoff (Carr & Head, 2015).

During the Hesperian period, approximetly 27 meters of GEL of water had been outgassed to the surface of Mars, but a more recent study found this number to be significantly lower at just 4.6 meters GEL. Similarly, for the Amazonian period, the initial estimate was 14 meters GEL, but a 2012 study found it to be 2.8 meters GEL (Carr, 1996; Greeley, 1987). Both studies made assumptions about the volume of volcanic rocks erupted and the water content of magmas, which was assumed to be 1%. However, that the actual water content of magmas is uncertain and can range from

0.0075% to 2.8% which in turn can affect the calculation of the water volume and the intial estiamtes of the near surface water (Carr, 1996; Greeley, 1987). Based on estimates of water outgassed during the Hesperian and Amazonian eras, Carr & Head estimate that 2.3 meters GEL of water was lost as a result of H2SO4 formation during the Hesperian period and 1.4 meters during the Amazonian period (Carr & Head, 2015).

Water loss to space over the last 3.5 billion years has been estimated to be a few meters, but this estimation is based on current loss rates of hydrogen. However, the hydrogen content of the atmosphere and the amount of water loss is also affected by the planet's tilt. Studies suggest that the water content in the lower atmosphere at an average tilt of 40 degrees could be much higher than present-day levels. The loss of oxygen to space may be a better indicator of water loss than hydrogen loss. It is estimated that up to 35 meters GEL could have been lost from the upper atmosphere over the past 3.5 billion years. It's assumed that this loss rate was constant, with 5m lost during the Hesperian period and 30m during the Amazonian period (Carr & Head, 2015). In the Hesperian, an additional 5 meters of water were gained from outgassing and 7 meters were lost to space and chemically fixed, leaving 64 meters of unbound water that must have been derived from other events in the Hesperian or carried over from the Noachian period. (Carr & Head, 2015).

Currently, The amount of unbound water at the surface of Mars is suggested to be 34 meters GEL. At the end of the Hesperian period, it is believed that a total of 62 meters of unbound water were present near the surface, with 3 meters gained from outgassing and 31 meters lost to space and chemically fixed in the ground during the Amazonian period (Carr & Head, 2015).

## 3.3 Geomorphological Evidence of Fluvial and Glacial Activity

### 3.3.1 Alluvial Fans

Alluvial fans are landforms that are formed by the depositing of sediment, typically by a stream or river, at the base of a mountain or cliff. They are usually fan-shaped and can range in size from a few meters to hundreds of kilometers across. The sediment that forms alluvial fans is typically transported by water, but can also be transported by wind or ice. These alluvial fans are found at mid-latitudes on Mars, and their presence suggests that there may have been periods of fluvial activity on the planet in the past. However, the origin of these alluvial fans is debated among several hypotheses, such as snowmelt versus rainfall, transient or stable climatic conditions, and the role of impact or volcanic activity in melting water ice (Blair & McPherson, 2009). Example of fan deposits is the four fan deposits identified within the Degana-A crater that cover the entire floor area. The fan deposits were also observed on the

floor of the larger Degana crater, particularly in the southwestern quadrant. The fans within the Degana-A crater have low gradients in the range of 2° to 4° and almost equal areas (Harish et al., 2021). The fans located on the floor of Degana crater did not show as many sharp distributaries as observed on the fans located within Degana-A. The fans in Degana-A, particularly fans f1 and f3 (Figure 3.5) exhibit surface textures with noticeable bedding/layered sediments. The fan deposits observed within both craters (Degana and Degana-A) are likely Amazonian (Michael, 2013).

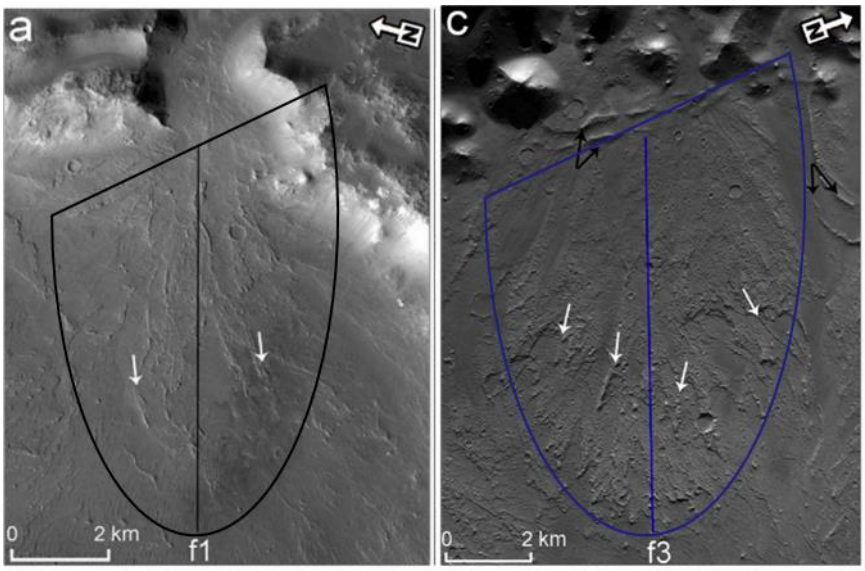


**Figure 3.5:** Fan structure and deposit distribution in Degana-A crater for Fan 1 (f1) and Fan 2(f2) (Harish et al., 2021).

Alluvial fans are often found on Earth in humid climates where there is a juxtaposition of high- and low-relief topography. The size and shape of the sediment-source drainage basin, as well as the mechanical properties of the sediment it provides, has a significant effect on a fan's morphology (Harvey et al., 2005). Two hypotheses were developed to explain the evolution of alluvial fans: the evolutionary hypothesis, which viewed fans as a transient feature forming early in the development of a landscape or as part of a long-term cycle, and the equilibrium hypothesis, which held that fans were in a state of dynamic balance where deposition and erosion were equal over some time scale. Modern research has focused on understanding the various factors that control the formation of alluvial fans, such as climate, hydrology, tectonics, and geomorphology (Harvey et al., 2005).

Martian alluvial fans are influenced by several factors such as flow processes, dominant grain size, and gravitational effects. The lower gravity of Mars affects fan channel gradients and sediment loads, with sediment loads being higher for equivalent discharge, channel dimensions, and gradient, and sand-bed fan channels having lower gradients (Moore & Howard, 2005). Based on the comparison of Martian alluvial fan morphometry to their terrestrial counterparts, The Martian fans are found to have

steeper gradients and lower concavity compared to the fine-grained alluvial fans of coastal California, but similar to the coarse-grained alluvial fans of the Basin and Range province. The available evidence suggests that the Martian alluvial fans are dominated by gravelly sediment (Moore & Howard, 2005).

### 3.3.2 Paleolakes

The surface of Mars has been shaped by both fluvial activity and impact cratering, and the interaction between these two processes can be observed in the formation of paleolake basins within impact (Goudge et al., 2015). On Mars, impact craters provide the dominant mechanism for creating basin topography, while on Earth, tectonics and glaciation are the main processes responsible for forming lake basins. Martian paleolake basins are commonly classified as either open-basin or closed-basin lakes. Open-basin lakes have an outlet valley that drains the basin and typically have at least one inlet valley as well, though there are instances of open-basin lakes forming without inlet valleys. Closed-basin lakes do not have an outlet valley and can only be filled and emptied through evaporation or seepage (Cabrol & Grin, 1999). Understanding the hydrologic setting of paleolakes on Mars is important for understanding the history and evolution of water on the planet.

#### 3.3.2.1 Closed-Basin Lakes

Closed-basin lakes on Mars are an important part of the Martian landscape, providing insight into the evolution of the planet's hydrologic cycle. These lakes, which do not have an outlet valley, are often contained within impact craters. An example of the closed basin lake is the lake located in the Gale crater (Figure 3.6). A study of 205 closed-basin lakes across the surface of Mars explored details about the morphology, morphometry, and mineralogy of these basins and associated sedimentary deposits (Fassett & Head, 2008). In order to be considered for the catalogue of closed-basin lakes, a basin had to have an impact crater or multiple merged impact craters as its boundary, at least one visible valley that breached the crater rim and flowed into the basin. The presence of an inlet valley indicates that the basin had some level of fluvial activity, but excludes basins that may have formed mostly through groundwater influx (Goudge et al., 2015). It is difficult to identify these types of basins in a global survey because they often lack visible signs of hydrologic activity. However, these groundwater-fed basins may still be an important part of the paleolake record on Mars. The length of the inlet valleys of each lake is analysed as a primary characteristic, with lakes being classified as having either short inlet valley under 20 km in length or long inlet valleys over 20 km in length. The length of the inlet valleys is likely influenced by factors such as the duration and strength of fluvial erosion, the slope of the valley, the surrounding topography, and the local geology.

The lakes with short inlet valleys correspond to the majority of lakes, tend to be concentrated in the Arabia Terra and Xanthe Terra regions, and may have been formed by groundwater (Cabrol & Grin, 1999). The distribution of these closed-basin lakes is similar to that of open-basin lakes on Mars. The lakes in the catalogue have a maximum combined volume of approximately 1.7 × 105 km3, or 1.2 m GEL. The catalogue also includes 55 closed-basin lakes with sedimentary fan deposits in their interiors. The lack of widespread evaporate deposits suggests that the lakes were too transient to undergo major evaporative concentration (Goudge et al., 2015).

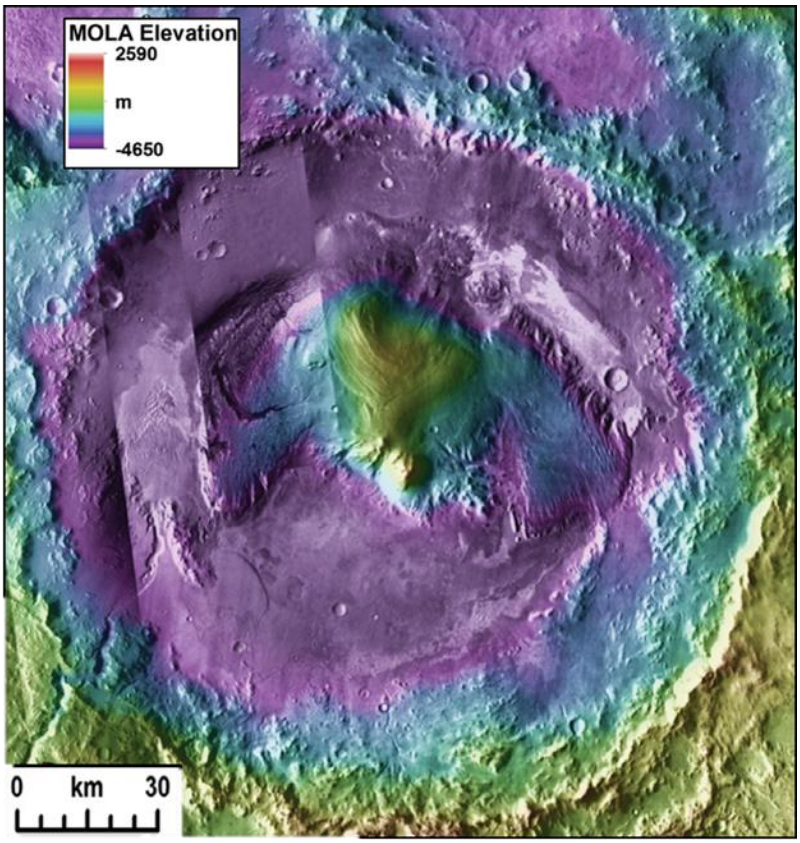


**Figure 3.6:** MOLA-Colored image of Closed-basin lake in Gale crater (Goudge et al., 2015).

#### 3.3.2.2 Open-Basin Lakes

High-resolution images from various Mars missions have been used to study the population of candidate lakes that were fed by valley networks and had clearly observed outlet valleys. It is identified as open basins (Figure 3.7). These valley network-fed lakes are believed to have been longer-lived and closer to equilibrium with the surface environment when they formed (Caleb I. Fassett & James W. Head III, 2008). The presence of an outlet indicates that a lake must have existed at the site. The minimum volume of these lakes is estimated using current topography, and the data on the input valley networks, elevations, and connections to other lakes are used to assess the amount of water needed to fill the lakes and the potential sources of water. The study

identified 210 open-basin lakes. The largest of these lakes, Eridania basin, is larger than the modern Caspian Sea that hold volume of more than 78,200 $km^3$ (Irwin et al., 2004).

The distribution of the lakes is partly affected by later geological events on Mars and that it is challenging to recognize open-basins in certain regions due to obscuring by younger geomorphological units. Additionally, there appears to be a weak inverse correlation between the volume of lakes and their elevation, with larger lakes being found at slightly lower elevations. Most open-basin lakes on Mars formed as part of connected lake-chain systems, with outlet valleys of these lakes crossing local drainage divides (Caleb I. Fassett & James W. Head III, 2008). These lake-chain systems were significant pathways for the integration of the surface hydrology of early Mars and were broadly consistent with drainage basins defined at the largest scale. It is noted that these lake chains were longer in length than most terrestrial systems and that the majority of the lake-chain systems were continuous over length scales of 200-600 km, but a few were longer than 1000 km(Caleb I. Fassett & James W. Head III, 2008). The study suggests that this is likely a result of the immaturity of the Martian landscape compared to Earth.

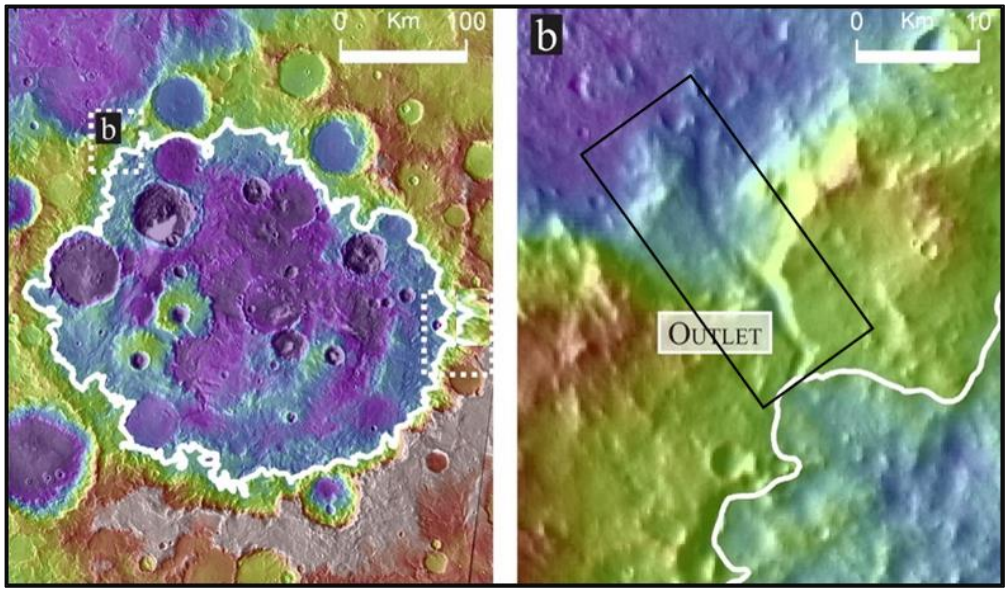


**Figure 3.7:** Example of large open-basin Lake on Mars with its outlet in Tikhonravov cratert (Caleb I. Fassett & James W. Head III, 2008).

It is suggested that groundwater was a net contributor to the filling of the large volumes of some lakes relative to their watershed in the Late Noachian. The presence of knobby material on the floors of some lakes supports the idea that groundwater played a role in their formation (Clifford, 1993). In addition, the water chemistry of potential groundwater-fed lakes may have been different from those fed predominantly by precipitation and that these differences may be preserved in the geochemistry and mineralogy in their lake sediments and may be detectable by orbital instruments (Irwin

et al., 2004). Additionally, many of these open basins connected to fretted terrain were potentially groundwater-fed, and a role for groundwater in these source lakes is consistent with sapping playing a role in the formation of some fretted valleys. The large volumes of some lakes relative to their watershed areas suggest that groundwater was a net contributor to their filling. Groundwater input may have been especially important for the largest lakes on Mars. The cataloged lakes in the study provide lower limits on surface water inventories, equivalent to a 3-meter-thick layer spread over the globe (M. C. Malin & Edgett, 2000). However, if the interpretation that regional-to-global-scale groundwater flow fed some of the lakes during the Noachian is correct, this implies that the subsurface water inventory was significant and that groundwater was not sequestered at great depths beneath a planet-wide cryosphere.

### 3.3.3 Impact Craters

The Gale Crater is believed to have formed due to an impact event that took place on the Martian crustal dichotomy. The impact caused a valley network that was active prior to the formation of Gale Crater to be partially buried. According to Irwin et al. (2005), the extensive regional drainage system that existed in the area prior to the impact could have provided the water needed for the construction of Farah Vallis, which is a large canyon entering the Gale Crater from the south. They suggested that this period of lake building occurred after the deposition and partial removal of Mount Sharp sediments by Aeolian erosion. Large lakes were detected in the Gale Crater in the past. However, the exact timing, extent, and duration of these lakes remain unknown. For example, one of these lakes is the Pancake Lake Stand. It is defined by the Pancake delta, which terminates at an elevation of −3280 meters, according to the HRSC contour (Blake et al., 2013).

In the southern highlands of Mars in the easternmost side of the Coprates quadrangle, there is an area characterized by a volcanic dome that extends over 200 km in diameter and is covered by impact craters of varying sizes. The largest crater on the western flank of the volcanic dome is the Degana crater, which has a diameter of 50 km and a depth of 2 km. Another impact crater within the Degana crater, named Degana-A, has a diameter of 20 km and a depth of 0.7 km (Figure 3.8). The dome and its surrounding region are mapped as Mid-Noachian highland units (Harish et al., 2021), which are formed by volcanic and impact activity and are moderately to heavily degraded with dense valleys, grabens, and wrinkle ridges (Xiao et al., 2012). A significant part of the crater rim was breached and this breach is associated with five valleys which originated from Degana's crater wall. Nearly all five valleys converge outside the eastern wall of Degana-A crater and breach this part to form the fan f1 deposits. Using a Poisson timing analysis, the age of the Degana crater estimated to be in the early Hesperian period (Michael, 2013).

Chukhung crater is located within the early-Hesperian volcanic unit and has a maximum bounding age in the early Hesperian period, around 3.59 billion years ago. It is proposed to be formed by fluvial or lacustrine processes, likely from precipitation or snowmelt. The upper incised plains unit is interpreted as fluvial deposits and the upper plains and ridges unit is proposed to be composed of resistant materials that formed within the upper layer of the fluvial deposits (Butcher et al., 2021). The presence of LDAs in Chukhung crater suggests the presence of ice-rich glaciers in the past (Holt et al., 2008). However, no similar ice-rich deposits are observed on the northern or eastern portions of the crater floor or wall, indicating a regional variation in the distribution of ice. This observation supports the idea that ice-rich glaciers were present in the past on Mars.

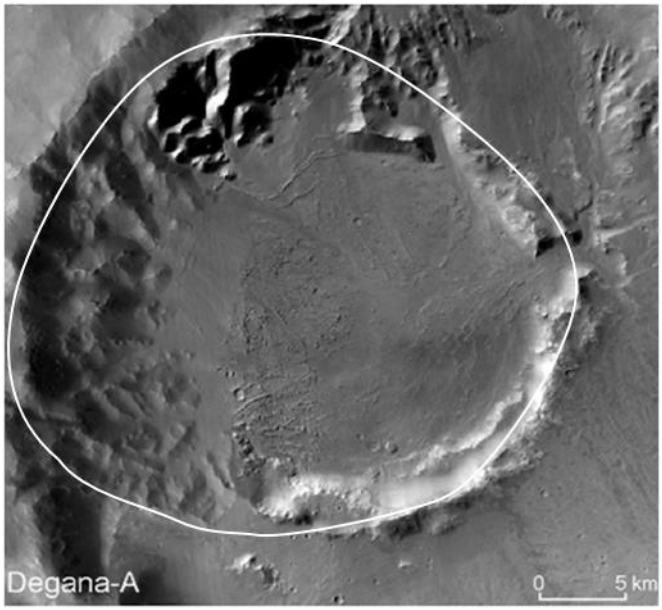


**Figure 3.8:** Examples of Craters (Degana-A crater) (Harish et al., 2021).

### 3.3.4 Pingos

Periglacial processes on Mars can create a variety of landforms, including thermal contraction polygons and pingos. Pingos are hills with an ice core that form when pore water in saturated ground is covered by an impermeable frozen layer. If the pore water is under sufficient pressure, it will push the permafrost surface upwards, forming an ice lens that freezes to create the ice core. Pingos can form through hydraulic or hydrostatic pressure, and their growth can continue for many decades (Burr et al., 2009). The presence of pingos on Mars could indicate the past or current presence of liquid water, which is of particular interest for understanding the origin of recent gullies believed to have been carved by water (Figure 3.9).

There are two types of pingos: open-system pingos and closed-system pingos. Open-system pingos form at locations with high hydraulic head, often on valley floors, while closed-system pingos typically occur in the shallow depressions of drained lakes. Both types of pingos are mounds that can be up to hundreds of meters in diameter and tens of meters high, with slopes typically less than 45 degrees. They are typically solitary features but may occur in clusters in some cases. Open-system pingos are more likely to be clustered than closed-system pingos (Cabrol et al., 2000). The overburden of a pingo is typically composed of frozen ground, while the core is made up of nearly pure ice. Fractures often form in the overburden due to tensile stresses during pingo growth, and if the overburden becomes thin and extensively fractured, the ice core may become exposed and begin melting. This can create a summit crater, which evolves into a shallow depression surrounded by a rampart once the ice core is completely lost (Dundas & McEwen, 2010) .

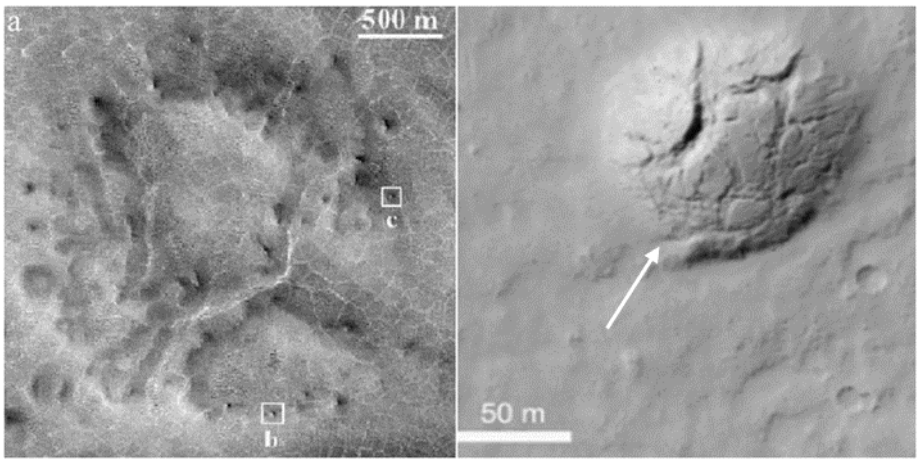


**Figure 3.9:** HiRISE image shows Evidence for pingos on Mars (Burr et al., 2009) and (Dundas & McEwen, 2010).

It is difficult to produce significant volumes of liquid water in the shallow subsurface of Mars in geologically recent times. The depth at which the temperature on Mars reaches 273 K (the melting point of water) depends on the thermal conductivity of the soil and is likely greater than 100 meters deep. High concentrations of salt can lower the melting point and reduce the depth to melting, but this requires salt concentrations of tens of weight percent (Dundas & McEwen, 2010). The presence of pingos, would indicate past occurrences of liquid water and the presence of currently extant ice.

The Athabasca Valles mounds on Mars have been proposed as pingos and they often have summit craters and little indication of fractures. This suggests they may have formed through a different process (Burr et al., 2005). A cluster of mounds on a crater floor on Mars has also been proposed as pingos, but these mounds are densely fractured. Further, flat-topped mounds have been observed on the Utopia plains on

Mars by the HiRISE camera. These mounds are often circular but may also have irregular shapes and steep sides. They have flat summit areas, which may be slightly domed or depressed, and are covered with small boulders similar to the local plains' material. In some cases, smaller conical mounds occur near the flat-topped mounds, but these generally lack visible fractures and may be capped by material of a different composition (Dundas & McEwen, 2010).

The minimum amount of near-surface water required to form a pingo, is the volume of the mound. If the driving pressure for the formation of the pingo is due to the freezing of near-surface water in porous, saturated ground, the minimum water volume required is an order of magnitude greater, because the driving pressure and excess ice volume are created by the expansion of freezing water (Dundas et al., 2008). The volume of ice required if a mound on Mars is a pingo can be compared to the estimated water volumes involved in the evolution of gullies on the planet. It is possible that mounds and gullies on Mars could have the same source of water.

### 3.3.5 Ridges

Arcuate or wide U-shaped ridges located over fans f2 and f3 in Degana-A crater was observed. They have characteristics consistent with moraines observed on Mars and varied thickness and height. These ridges are superposed on the fan deposits and are oriented differently from the fan deposits. Additionally, the thickness of the ridges and the calculated ratio of basal stress to density suggest that these ridges could have formed by glacial activity (Harish et al., 2021). The "esker vs. inverted paleochannel problem" refers to the difficulty in distinguishing between features on Mars that were formed by the erosion of a river channel (inverted paleochannels) and those formed by the erosion of a glacier (eskers) (Williams et al., 2013).

The sinuous ridges within the Chukhung crater are suggested to be inverted valley-interior channels and the isolated pockmarked unit is thought to possibly be an airfall deposit (Figure 3.10). The N1 (located in the northern floor of the crater) ridges are interpreted as inverted paleochannels, formed by the erosion and infilling of original valley channels. The alignment of N1 ridges with valleys and the presence of possible resistant materials within the upper plains and ridges unit support this interpretation. The rugged surface textures and variable crest morphologies of the N1 ridges suggest that they have undergone significant erosion and degradation since their formation (Butcher et al., 2021). The N2 ridges, which are not clearly associated with valleys and have a different morphology, may also be inverted paleochannels, but their origin is less certain (Butcher et al., 2021). The absence of evidence for past or present glaciation on the northern floor of Chukhung crater supports the interpretation that the sinuous ridges are of fluvial rather than glacial origin. They have variable lengths and sinuosities, with more rugged surface textures than other sinuous ridges in the crater.

They have variable topographic expression, ranging from prominent ridges to low-relief features and have typical heights of 5-20m and widths of 150m-1.1km.

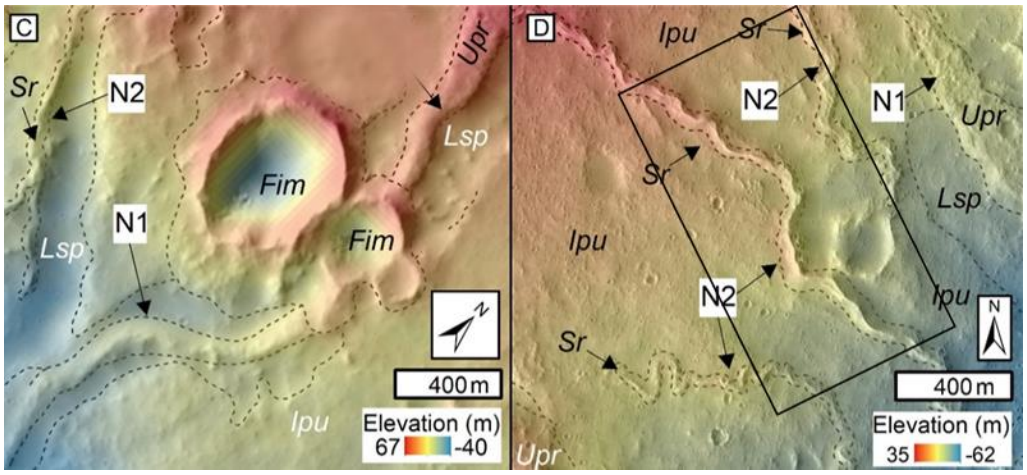


**Figure 3.10:** Sinuous ridge on the right picture and Sharp-crested ridges in the left picture in the Chukhung (Butcher et al., 2021).

### 3.3.6 Polygonal Pattern

Polygonal-shaped features were noticed within the Degana crater and on the fan deposits (Harish et al., 2021). These polygonal patterns are observed primarily on the fans in Degana-A, and also on the inner and outer eastern wall of Degana-A crater. The majority of polygons' boundaries or fractures observed on the fans appear irregular, whereas polygons over the Degana-A walls visually appear regular or organized to each other (Figure 3.11). These polygons are 10s of meters wide and the fracture length varies accordingly. Over the fans, most of the polygons are negative relief features, and polygons on the wall of Degana-A are distinct from the polygons observed on the fans, in terms of the slope at which they formed (Harish et al., 2021). The polygons on the fans suggest a potential involvement of volatiles (potentially ice or adsorbed water in clay minerals) in their formation, which would imply a periglacial environment postdating the deposition of the pile of sediments.

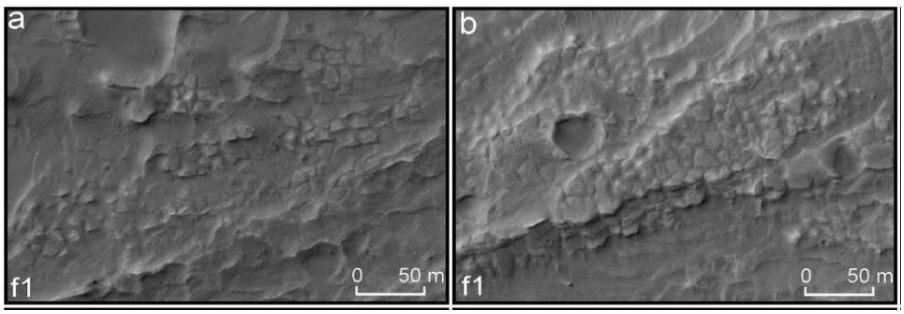


**Figure 3.11:** Polygon patterns in fan 1 in Degana-A crater, a) polygons of Trough boundary type and b) Polygons located over the layered ridges (Harish et al., 2021).

# 4 Methodology

## 4.1 Study Site

To conduct this study, a specific site located in the northeaster part of Mars' southern hemisphere was selected. This area was chosen due to its abundance of unique geomorphological features, which are more prevalent in the southern hemisphere compared to the relatively flat northern hemisphere. In addition, it is close to other key areas discovered on Mars. The site location, geological characteristics, and boundaries were carefully identified and will be presented in detail in the following section. To analyse the geomorphology of the site and calculate relevant morphometric data, a rigorous methodology was applied, which will also be thoroughly explained in this study.

### 4.1.1 Location

Our site of interest corresponds to a basin, located in an area that was affected by various geomorphological process, as it is located in a highland area norethern to Terra Cimmeria. This area is believed to have formed in the Middle Noachian, and it is also adjacent to a Late Noachian highland and an Amazonian and Hesperian impact crater such as Gale crater (Tanaka et al., 2014a). The site was located in the southern east of Mars within the following coordinates 133.228 - 127.9 Longitude, and - 5.439 to -11.096 Latitude with an approximate area of 46957 $Km^2$ (Figure 4.1). The valley network suggested to empty in an area formed in the transition zone between Hesperian and Noachian (Tanaka et al., 2014a). This suggests that the site could have been shaped by a variety of geomorphology processes, including water-related processes such as erosion, sedimentation, and possibly the formation of paleolakes.

In order to determine the presence of water-related landforms and associated activities, a detailed geologic survey of the target area is imperative. This entails mapping and analyzing surface features through remote sensing observations to gather supplementary data that can aid in identifying and comprehending the processes responsible for shaping the region, and to detect any signs of past water activity. The data acquired is then subjected to morphometric analysis and compared to existing literature, enabling insights into the Martian climate and geologic history. Such an investigation would contribute to our understanding of the planet's geological evolution and the role played by water in shaping its surface features.

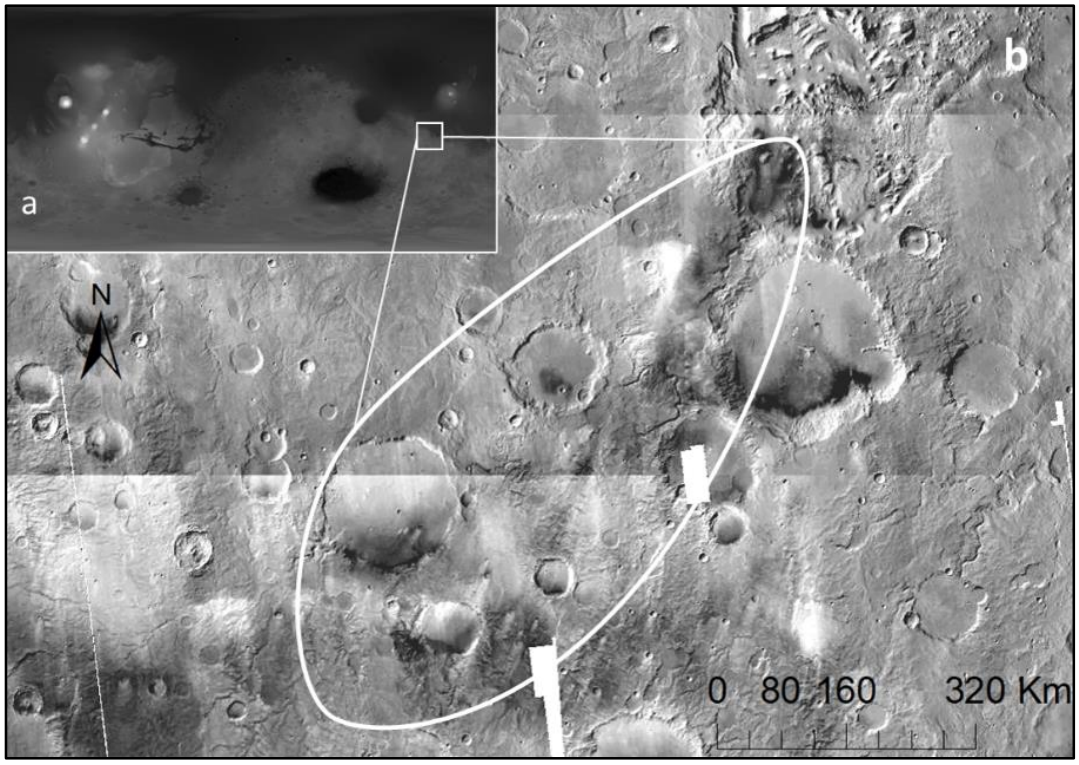


**Figure 4.1:** Area of inspection in mid-latitude regions on Mars, a) shows the image of Mars surface obtained by MOLA and b) the area understudy shown by ArcGIS and obtained by CTX mosaic data.

### 4.1.2 Geomorphological Characteristics

The Middle Noachian highland unit (mNh) is found in regions where the Early Noachian highland unit (eNh) is rare or absent, and it forms low-lying surfaces that are adjacent to higher-standing eNh outcrops. Middle Noachian impact basins, with diameters greater than 150 km, are also present in the highlands (Tanaka et al., 2014b). The adjacent geographical region is described as Hesperian and Noachian transition unit (HNtu) which represents the transition between the Noachian and Hesperian periods and preserves evidence of early Martian processes and the transition from a more active to a more passive geologic period (Tanaka et al., 2014a).

The site occurs northern to Terra Cimmeria which is characterized by high-standing plateau-like landforms, with a heavily cratered surface and evidence for channel presence (Figure 4.2). It is detected by Mars Reconnaissance Orbiter (MRO) mission which is a spacecraft launched by NASA in 2005 and is currently still in operation. Its main objective is to explore and study the surface of Mars in greater detail, as well as to serve as a communications relay for missions that land on the planet (Adeli et al., 2016).

In Terra Cimmeria, the fluvial system is composed of three sections: upstream, intermediate, and downstream. The model absolute age of the bedrock unit in the intermediate section shows an age of 1.8 + 0.2/-0.2 Ga, indicating the maximum age of fluvial activity. Along the main channel path, narrow valleys are observed that resemble Amazonian-aged glaciofluvial valleys, which may be related to ice-rich deposits in mid-latitude regions. The presence of a 5 km-wide deposit at the eastern channel head may suggest that it is a remnant of a wider ice-rich deposit that partly melted in the past and incised the narrow valleys (Adeli et al., 2016). Alternatively, it may reveal a long history of re-deposition and disappearance of glacial deposits in the past. Local depressions located at the head of the narrow channels may have hosted ice or snow deposits that entirely melted and carved the narrow valleys toward the main water stream. Terra Cimmeria's morphology presents a strong indication of water's existence on Mars, owing to the presence of various landforms that suggest the past activity of water.

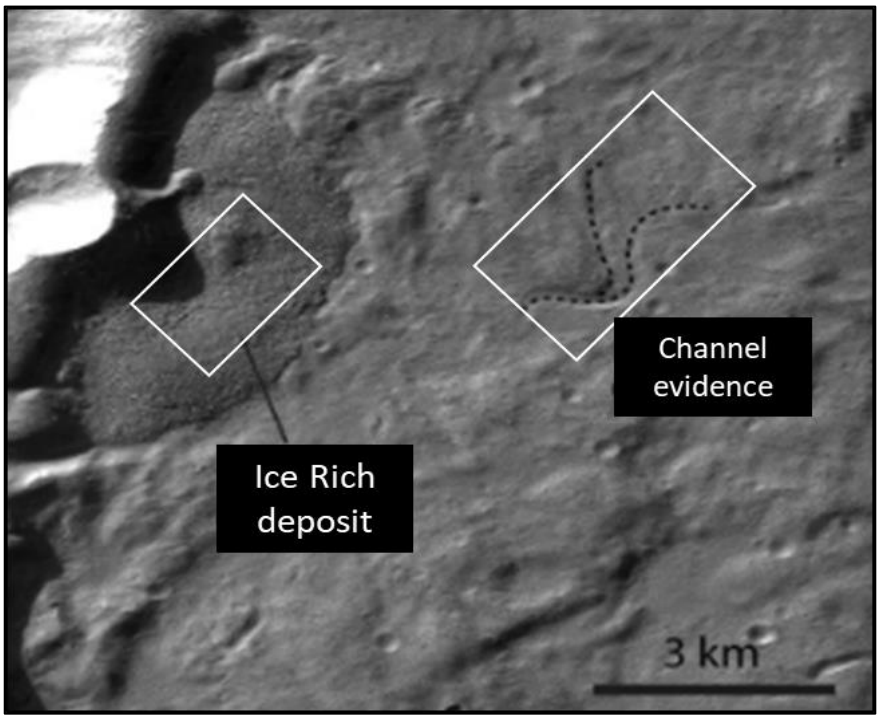


**Figure 4.2:** The water related landforms in northern of Terra Cimmeria shows possible structure of Ice rich deposit and an evidence of channel (Adeli et al., 2016).

The gale crater (Figure 4.3) is found 240 km away from the site of interest. It is the location of landing by the Mars Science Laboratory Curiosity rover. It is a large impact crater on the surface of Mars, located in the southern hemisphere of the planet, near the equator (Blake et al., 2013). The diameter of Gale Crater is about 154 km, and it has a central mountain, called Mount Sharp, which rises to a height of about 5.5 km above the crater floor. It is believed to have once a large lake, and the evidence of this past habitability is preserved in the sedimentary layers that make up Mount Sharp

(Palucis et al., 2016). The rover has been exploring the crater and its surroundings since it landed on Mars in August 2012. The major depositional and geomorphic events (deposition of delta/fans and constitution of the mound) in the carter are suggested to be ended by around 3.3 to 3.5 Ga and since then, most modifications have been due to wind erosion. Hence, the valley system of the Gale was dated to Late Noachian to Late Hesperian (Tanaka et al., 2014b).


**Figure 4.3:** The distance between the study area and Gale crater, Geologic Map of Mars (Tanaka et al., 2014b)

The crater has a delta and several small inverted channels on the southern flank of Mount Sharp which terminate at this elevation. A lake which was identified at this elevation would have covered a surface area of 5832 $km^2$ and would have had a mean depth of 0.7 km, assuming that Mount Sharp was at its current extent and that the crater floor had not undergone significant erosion or infilling since that time. This would have given the lake a volume of 3780 $km^3$ (Palucis et al., 2016). Understanding the geomorphology of this crater is a matter of importance due to its close to the study area and part of its valley is suggested to be formed within the same period as the valley network in the study area that interacts and influences the geomorphology of landforms within the area.

## 4.2 Satellite data

The identification and study of geological structures on Mars rely primarily on satellite images obtained from various missions and satellites equipped with advanced technologies. The resolution of these images is a critical factor in accurately depicting the surface of Mars and conducting precise calculations of elevations and slopes of the terrain, which are essential in visualizing and identifying the landforms present. Various satellite missions have contributed to the collection of high-resolution images of the Martian surface, such as the Mars Reconnaissance Orbiter (MRO), which has provided images with a resolution of up to 25 cm per pixel. These high-resolution images allow for the identification and detailed analysis of geomorphological features on the Martian surface, such as craters, valleys, lakes, and other landforms, which can provide valuable insights into the planet's geological evolution and the processes that have shaped its surface over time (M. Malin, 2022).

The CTX (Context Camera) data refers to photographs taken by the Context Camera on board the Mars Reconnaissance Orbiter spacecraft (MRO). The MRO sent into space in 2005 and has been orbiting Mars since 2006, providing detailed observations of the planet's surface and atmosphere. The CTX camera is positioned 400 kilometres above Mars and has a resolution that can reach 6 meters per pixel, capturing images that show a 30-kilometer-wide view of the Martian terrain in grayscale. The images are joined together to form mosaic that covers the martial surface. The produced images are of high-resolution images which is important for studying various geological features and mapping the distribution of rocks and minerals on the planet (M. Malin, 2022). The CTX data is publicly accessible through the Planetary Data System, which is a repository of data from NASA's planetary missions. The data source is *esri* online webpage.

MarsSi is a product from a French institute that offers for users efficiently select observations, process raw data using automated pipelines, and receive final products that can be visualized in GIS software such as ARCGIS and QGIS. Additionally, it offers an automatic stereo-restitution pipeline that creates Digital Terrain Models (DTMs). They provide CTX stereo dataset which consists of High-resolution pictures. The CTX stereo is constructed by two CTX images for the same area that captured from slightly different angles, which produce a stereo image demonstrate the terrain of Mars. A primary objective is to acquire about 1000 stereo pairs of images to create Digital Elevation Models (DEMs), which allowed scientists to calculate the thickness of Martian features with greater precision (MarsSi, 2022). They are also used to calculate more accurate measurements such as the slope of the alluvial fan and to draw a contour map to analyse the radial profile of the alluvial fan.

To obtain data from MarsSI, the first step is to register on their website and search for the required data, such as MOLA or CTX. If the data is available for the desired area, it can be downloaded directly. However, if the data is not available and requires processing, a request can be submitted through the website. It is important to note that the processing of the data may take some time, and the processed data will be made available for download after a few days based on the requested data (MarsSi, 2022).

The CTX camera works in conjunction with other instruments, such as the High-Resolution Imaging Science Experiment (HiRISE) and the Compact Reconnaissance Imaging Spectrometer for Mars (CRISM), to enhance the quality of images taken of Mars. The HiRISE camera is able to capture high-resolution images up to 30cm per pixel. Starting from November 2006, HiRISE, was able to capture detailed images, visualize small objects and obtain colour data over 20% of the field of view. The HiRISE images demonstrate high resolution images that can give much more information about the geology of Mars (McEwen, 2022). A small part of the area of study was part of an obtained HiRISE image and it will be presented in the study to emphasize the role of HiRISE images. The image is obtained from the online website.

The Mars Orbiter Laser Altimeter (MOLA) digital elevation model (DEM) is a topographical mapping instrument that was part of the Mars Global Surveyor Mission (MGS), which was launched in 1996 by USA. The MOLA instrument used laser ranging to measure the distance from the spacecraft to the Martian surface and create a high-resolution 3D map of the planet with resolution of 463 m/pixel at lower latitudes to 115 m/pixel near the poles. MOLA also can measure the radiance of the Martian surface at a wavelength of 1064 nm since it functions as a passive radiometer. MOLA was used to access and analyse available datasets in order to study the surface features of Mars (MarsSi, 2022). In addition, it was used to validate the detected landforms from the CTX images such as the craters, lakes, and alluvial fans by observing the difference in elevation.

The ArcGIS software is a geographic information system (GIS) that was created by esri. It allows enables users to work with a wide range of tools and functions that can process and analyse raster and satellite data. One of the key features of ArcGIS is its ability to create shapefiles that allow for the visualization and highlighting of structures and characteristics based on geographic locations and maps, making the interpretation of data much easier and efficient (ESRI, 2012). While R studio is an open-source programing tool used in data analysis and interpretation. It provides a user-friendly interface that allows for efficient coding, debugging, and visualization of data,

specially methods for data representation and graphing with some packages and functions such as “dplyr” and “ggplot” that are used to create the figures related to the area elevation and slopes (RStudio Team, 2020).

MOLA, CTX and HiRISE are the most recent and advanced instruments that have provided us with a vast amount of data about Mars. These data sets contain valuable information that can be analysed to gain deeper insights about the planet's geological history and its atmosphere. The data are used incompatible with other software such as ArcGIS. We used to visualize and utilize the data collected by MOLA and CTX stereo. ArcGIS desktop along with R studio are used to create the figures that demonstrate and analyse information about Mars geology. The utilized satellite data about Mars are listed in Table 4.1.

**Table 4.1:** Information about satellite data used for analysis of Mar's surface geology

| **Data** | **Resolution** |
|---|---|
| CTX | 6 Meter / Pixel |
| HiRISE | Up to 30 cm/pixel |
| MOLA (DEM) | 463 Meter / Pixel |
| CTX stereo | 12 Meter/ pixel |

## 4.3 Landform Detection and Measurements

The data obtained from CTX mosaic, CTX stereo and MOLA were visualized using the Geographic Information System (GIS) software ArcGIS, in order to explore the region of interest and identify various geomorphological features that could have been shaped by a combination of geological and climatic activities. The primary objective of this study was to pinpoint the landforms that could have been created by flow of water within the area. After identifying special characteristics landforms, they are delineated based on the image of CTX mosaic. Then, it was represented in polygonal shapefile to be used for further analysis process. Morphometric calculations such as area, slope, and elevation were performed using the advanced functions available in the ArcToolbox Data Management and Spatial Analyst tools in ArcGIS for conducting calculations in Raster. Several landforms have been detected within the area of interest, and their characteristics and geology were thoroughly investigated, with particular attention paid to the nature of their formation and evolution. The reference for valley networks that connect the landforms and interact with them, the martial valley database used by (Alemanno, 2018).

Alluvial fans are identified from the CTX mosaic image based on their description as a geomorphic landform that exhibit a distinctive fan-shaped structure which may be produced by the deposition of sediments transported by water as it flows from a confined channel to an open basin. To better comprehend the sedimentary characteristics of these features on Mars, the volume, area, and radius of alluvial fans were calculated, and analyses of radial and cross-fan profiles were conducted. The area calculated based on the polygon area. Furthermore, a comparative analysis was undertaken between the Martian fans and their terrestrial analogues, with the aim of elucidating the differences in their characteristics. This comparative analysis allows for a better understanding of the formation, morphology, and sediment characteristics of Martian alluvial fans. The slope, aspect and contour were calculated in ArcGIS from *the arcToolbox → Spatial Analyst Tools → Surface → 1) Aspect, 2) Contour, 3) Slope* as shown in (Figure 4.4).

The Volume calculated by multiplying the mean elevation by the area of the alluvial fan. The mean elevation is calculated based on the CTX stereo DEM in ArcGIS and MOLA DEM, where the reference point is identified as the lowest point in the fan. The absolute elevation calculated by ssubtracting the minimum elevation from the mean elevation. Then, the absolute elevation was multiplied by the area of the polygon. Another method was used to confirm the volume result is as following: after obtaining the absolute digital elevation model raster layer for the alluvial fan, the volume of it was calculated on pixel basis. The area of the pixel is multiplied by the elevation value of each pixel. Then, summation for the pixel volume will be calculated. This method is calculated in R studio.

In addition, the mean elevation over the alluvial area was calculated from summary statistics without being referenced. The minimum, maximum and mean of the slope and elevation was obtained using R programing. The slope and elevation layers obtained from ArcGIS were loaded to R Studio and the values of the elevation and the slopes were obtained. The radius of the fan and the distance between the sediment layers were calculated using the measurement tool. The fan radius was measured from the apex to the edges of the fan. The distance between the sediment layer was measured as they move from the apex based on their direction. The fan special structures were drawn using the edit session and create feature tool in ArcMap.

We searched for the presence of lake structures, which were differentiated into two categories: open-basin lakes and closed-basin lakes. An open-basin lake is characterized by the presence of both inlet and outlet valleys, whereas a closed-basin lake is recognized by the presence of only an inlet valley in addition to being part of impact crater. The shape of the lakes was studied, and the length of the inlet valleys was calculated and compared with the existing literature. The calculation of length of the inlet

is done using the measure tool in ArcGIS (Figure 4.4). The measurement begins at the edge of the lake and continues towards the end of the inlet. If there are multiple inlets, each one is measured, and continuous inlets are terminated when they show signs of disappearing or no longer connecting with the valley.

The volumes of the lakes, along with their relationship with the valley, was also determined. The slope of lakes was calculated in ArcGIS from the *arcToolbox* → *Spatial Analyst Tools* → *Surface* → *Slope* as shown in the third step in (Figure 4.4). The Volume calculated by multiplying the mean elevation by the area of the alluvial fan. The mean elevation is calculated based on the MOLA-DEM layer in ArcGIS where the reference point is identified as the lowest point in each lake. Then, the mean elevations over the lakes were calculated using R to see the potential volume for the lakes. The area of the lakes was calculated based on the area of the polygon from "calculate geometry" window and the unit were by $Km^2$ (Figure 4.4). In addition, analysis of the structure and morphology of the lakes was conducted and a comparison between them are made. The lakes also were compared to other lakes that are found on Mars surface.

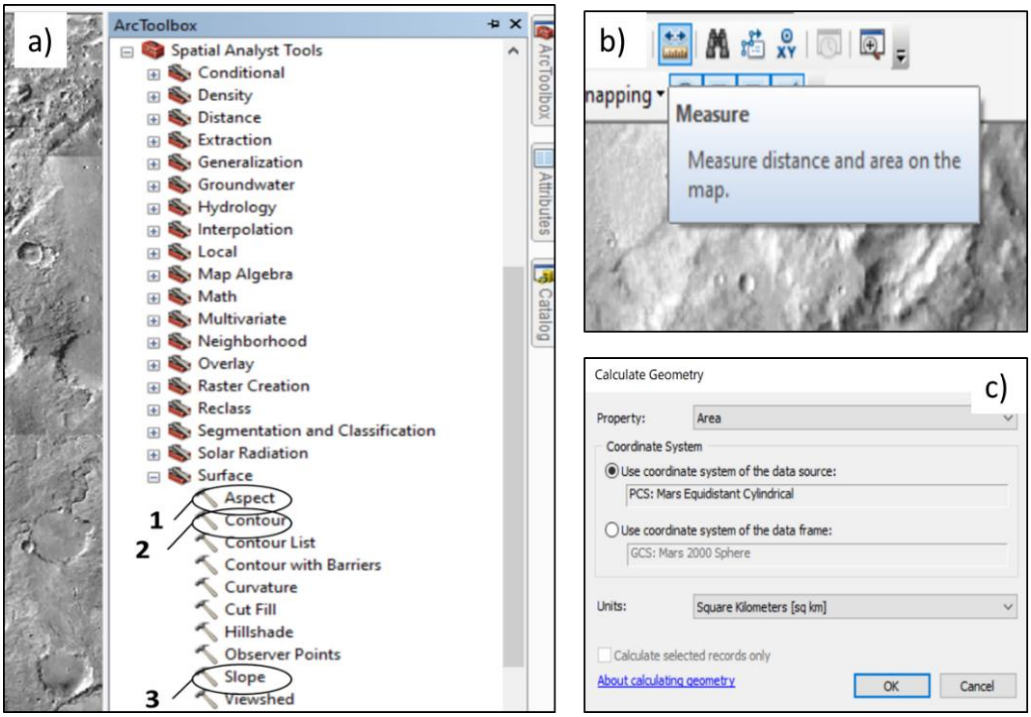


**Figure 4.4:** The functions used to carry out the analysis of data obtained using ArcMap, a) shows the ArcToolbox for calculating, slope and aspect, b) the measure tool to calculate distances, c) the calculate geometry to calculate area and coordinates of the polygons.

In addition to the identification of alluvial fans and lakes we conducted a thorough investigation of impact craters that are linked with the valley in the area of interest. A comparative analysis of their shape and area was conducted with reference to other craters, such as the Gale crater, Chukhung crater, and Degana crater, as documented in existing literature. The characteristics of the craters, including their elevation, morphology, and geological attributes, were recorded to gain a more comprehensive understanding of the geological history and processes of this region. The diameter of the craters was calculated based on the measure function in arcMap. The morphology and structures inside the craters were also investigated and compared with literature. The craters was calculated based on the measure function in arcMap. The morphology and structures inside the craters were also investigated and compared with literature.

The morphology of a crater on Mars, specifically its size and shape, provides valuable insight into the process that led to its formation. Smaller craters are ubiquitous on the planet and often display regular shapes, whereas larger craters tend to have circular, irregular shapes that are most likely caused by impacts. These larger craters are often linked to the flow and formation of water. In addition to shape, the size of the crater is also a useful criterion for distinguishing between the two types. Those with an area below 10 $km^2$ are classified as small craters, while those larger than this threshold are considered to be of the larger type to help in interpertation of the results.

Moreover, exploring the connection between landforms, polygonal structures, and the presence or absence of water becomes an essential task. To this end, an investigation of other structures such as pingos, ridges, and other polygonal structures was conducted. These structures may indicate the presence of liquid or ice water near the surface, providing valuable information about the geological time scale of the area. The structures of these shapes were recorded such as the shape of the feature, the number and its connection to the calley channels. In addition, their width was measured. The width was calculated from the measuremnt tools in ArcGIS. To further analyze their existence and their relation to water, additional analytical measurements were carried out. Their structure and morphology were compared with other highland observed within the area understudy.

# 5 Results

## 5.1 Study Area

Data obtained from MOLA was used to calculate the slopes and elevation of the area. The slope is shown to range between 0° and 31.98° with mean slope equal to 3.075° while the elevation ranges from -2265 to 3021 m with mean elevation of 1375 m. The region being studied exhibits a diverse range of geological landforms, many of which are potentially related to the surrounding valley network. These include the presence of paleolakes, craters of various sizes, and alluvial fans, among other distinct formations that offer crucial insights into the past history of Mars. By examining these geological features and their relationships to one another, we can gain a more comprehensive understanding of the complex geological processes that have shaped the Martian landscape (5.1).

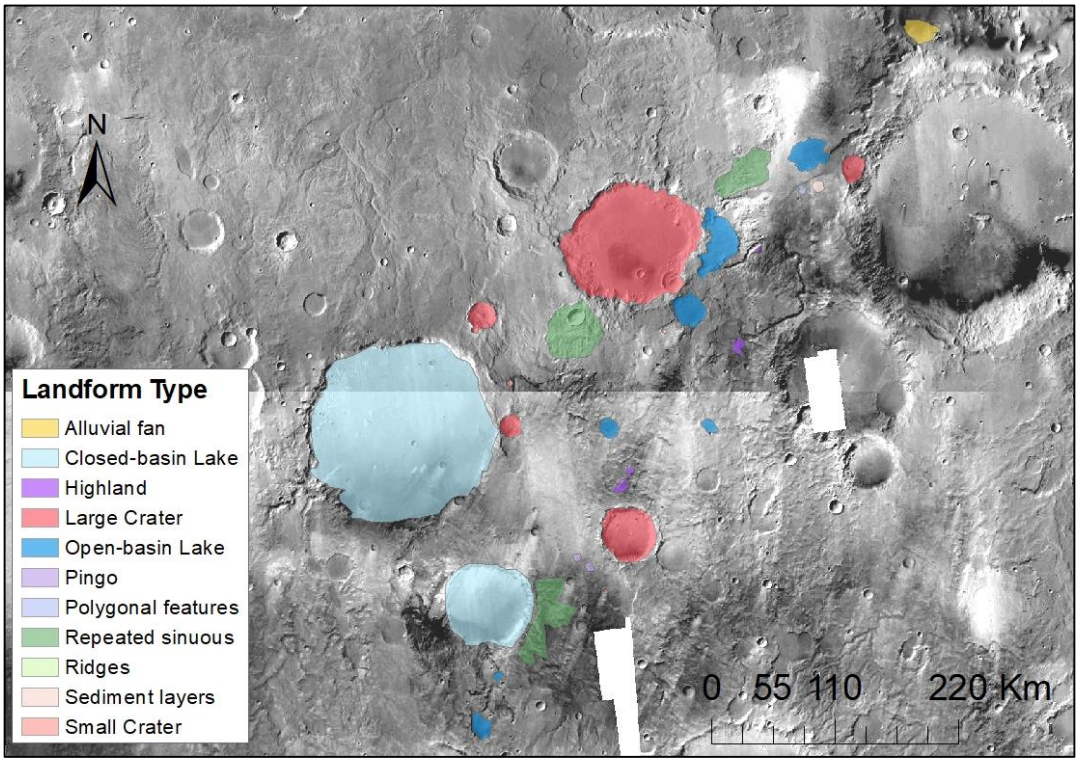


**Figure 5.1:** Identified Landforms from CTX mosaic image in ArcGIS northern Terra Cimmeria

## 5.2 Alluvial Fan

An alluvial fan was detected in 132.8, -5.106 Decimal degrees. The area of the alluvial fan in question is approximately 129.2 square kilometers, making it a relatively large fan (Figure 5.2). The fan exhibits an elevation range from -2312.3 meters to -1782.3 meters, as calculated from the CTX stereo data (Figure 5.2). Notably, the fan's mean elevation, after referencing the lowest point as the benchmark for other points, hovers around 200 meters, differs from the MOLA-DEM data, which records the mean elevation as 133 meters. The gradual slope from the apex to the periphery of the fan is represented in the contour map of the area, also featured in the figure. Notably, the MOLA-DEM data revealed that the slope ranged from 0.44° to 7.8°, with an average slope of 1.9°. Whereas higher resolution images from CTX stereo data revealed that the slope ranged from 0.2° to 40°, with a mean slope of 8°. The slope distribution graph in (Figure 5.3), indicates a leftward skewness, with the majority of values situated below 20°.

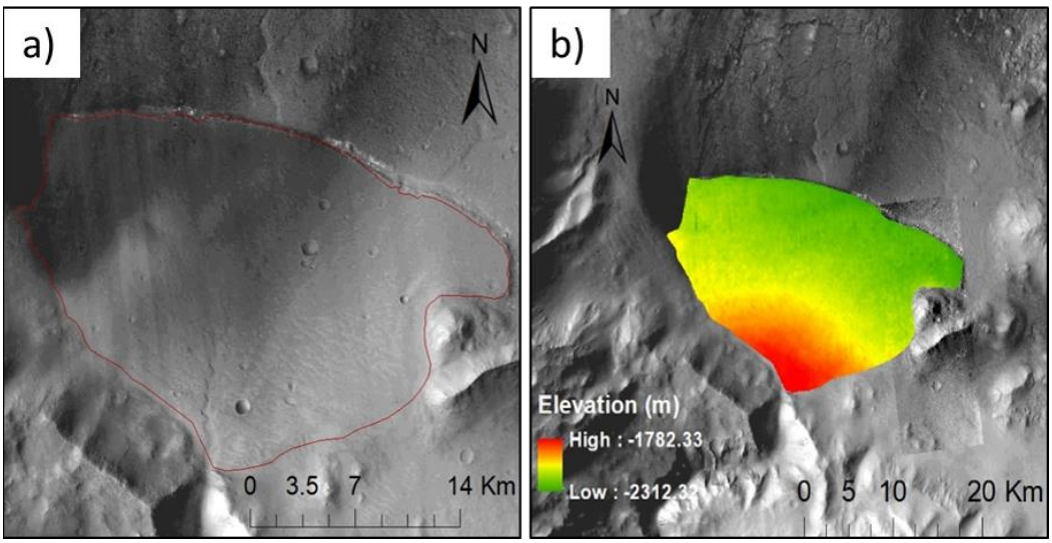


**Figure 5.2:** Identified alluvial fan in the top of the area of interest obtained from CTX mosaic, a) shows the alluvial fan, b) shows the elevation range within the fan from CTX stereo.

The potential volume of sediment that could be carried by the fan is estimated to be between 17.18 which obtained by MOLA-DEM data to 25.84 $Km^3$ that is obtained by CTX streo data. The value of the volume of the alluvial fan which was calculated based on pixel area and elevation value equal 25.86187 $Km^3$. The volume of fan indicates that it is capable of carrying a significant amount of sediment. The radius of the fan is about 11 kilometers, which is a relatively large length for an alluvial fan. The gradual decrease in elevation towards the edges of the fan allows for a clear radial profile of the fan to be observed. Notably, the flow of sediment is primarily directed to the north, with a slight deviation to the east and west on the right and left sides, respectively (Figure 5.4). The distribution and direction of sediments reveal the

existence of two main lobes in the fan indicating the flow was more intense in the left side which is identified in Figure 5.5.

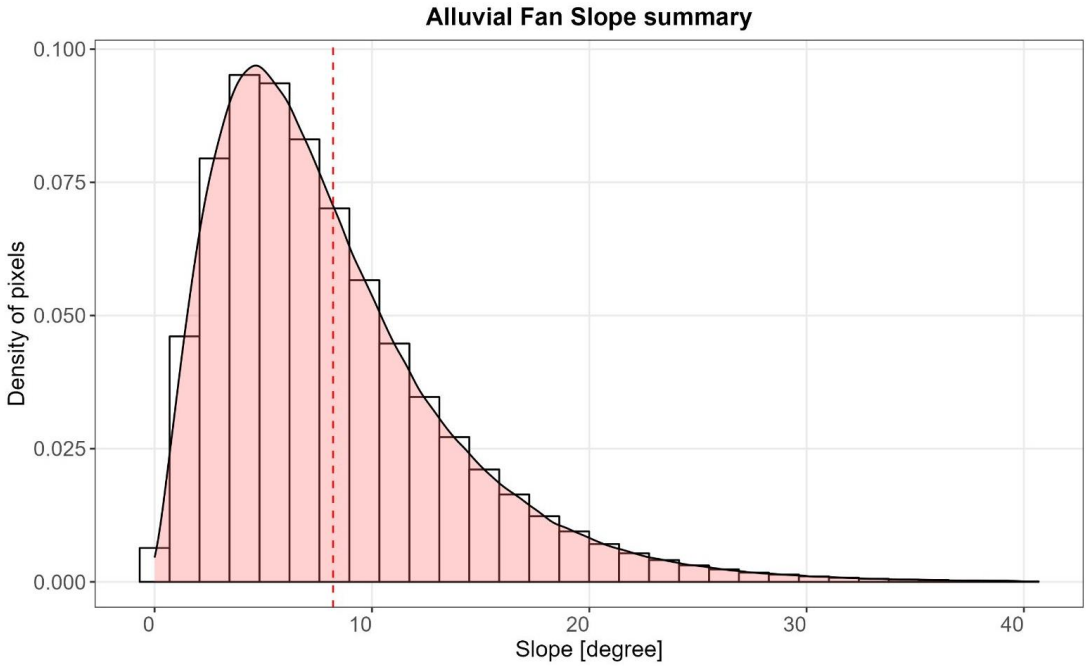


**Figure 5.3:** Density distribution of the slope of Alluvial fan per pixel.

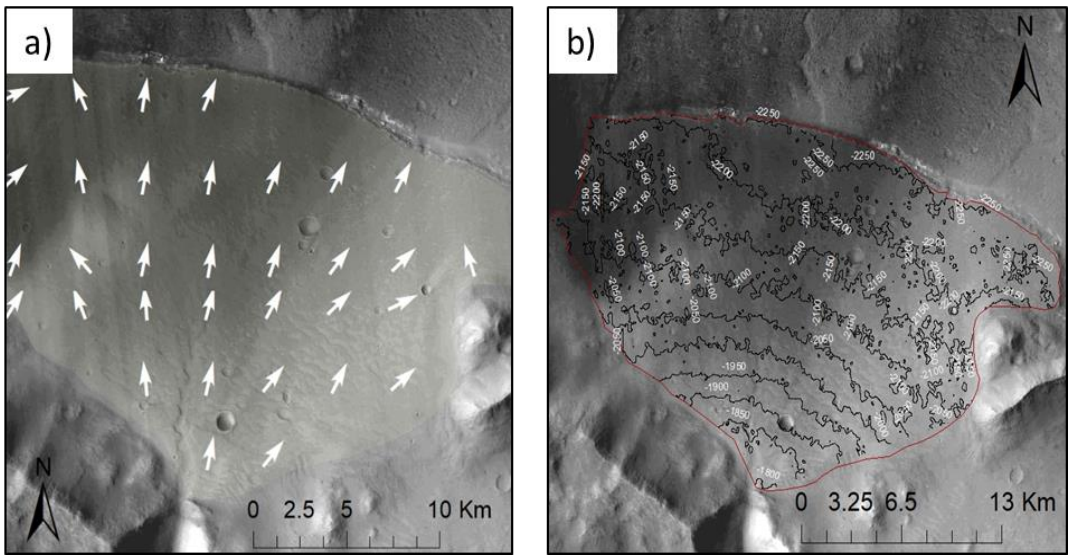


**Figure 5.4:** Capture of alluvial fan, a) the white arrows represent the direction of slopes or the aspect, b) shows the contour lines and the change in elevation (the grey map from CTX mosaic, and the arrows and contour lines calculated from CTX stereo)

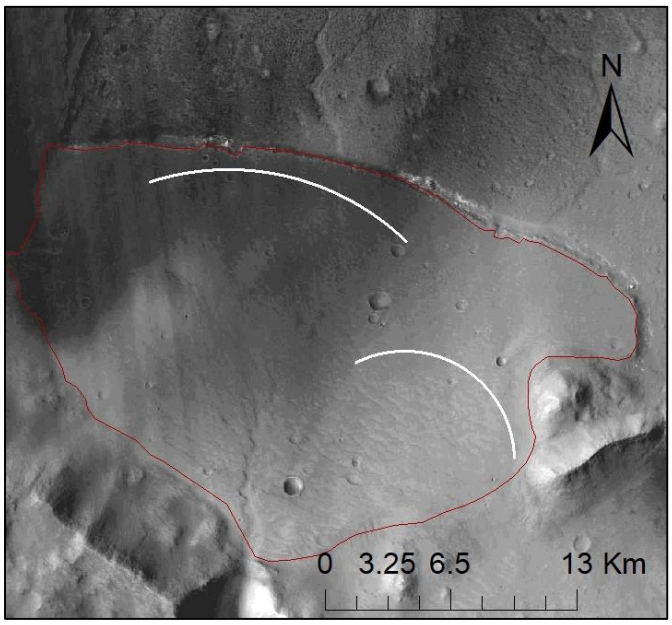


**Figure 5.5:** The potential lobes(white lines) formed by the sediments' deposition in the fan.

Another image used in inspecting the alluvial fan is the HiRISE image showed better visualization to the sediment layer compared to the resolution of the CTX mosaic image. However, within the area of interest only small part of the alluvial fan is available with HiRISE image, limit the inspection and analysis of other landforms in the area of interest (Figure 5.6).

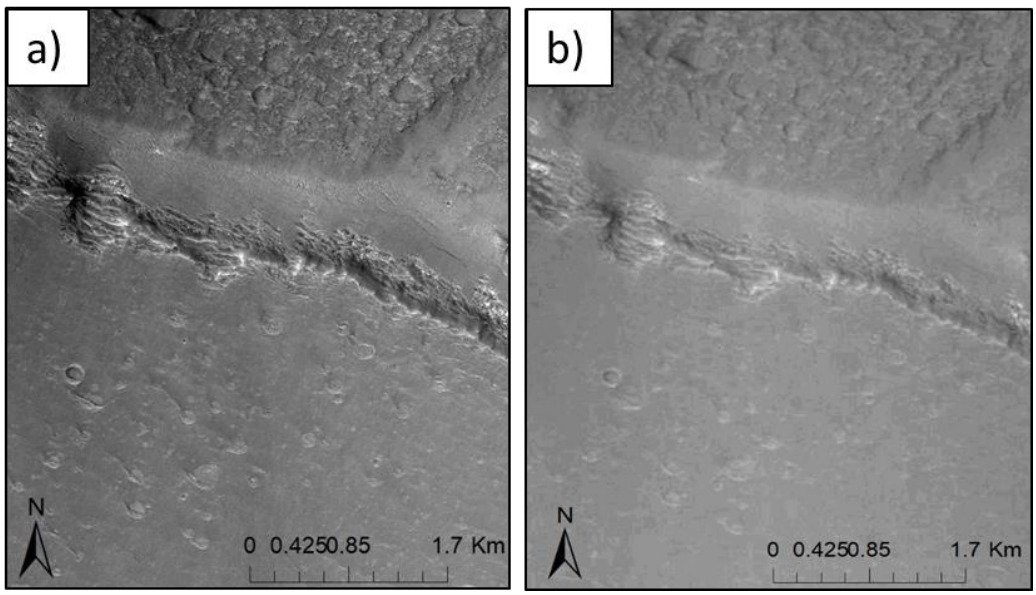


**Figure 5.6:** Part of the Alluvial fan shown by a) HiRISE image, and b) CTX mosaic image.

## 5.3 **Paleolakes**

Using high-resolution CTX mosaic images, the study identified a total of nine lakes in the area of interest. Among these, seven were classified as open-basin lakes, while the remaining two were closed-basin lakes. The open-basin lakes were identified based on the presence of an outlet, while the closed-basin lakes were identified by the lack of any visible outflow channels. The geographic coordinates of each lake and other geological structures are presented in Table 2 in the appendices section. Detailed images of the detected lakes are provided in (Figures 5.7 and Figure 5.8) for open-basin and closed-basin lakes, respectively.

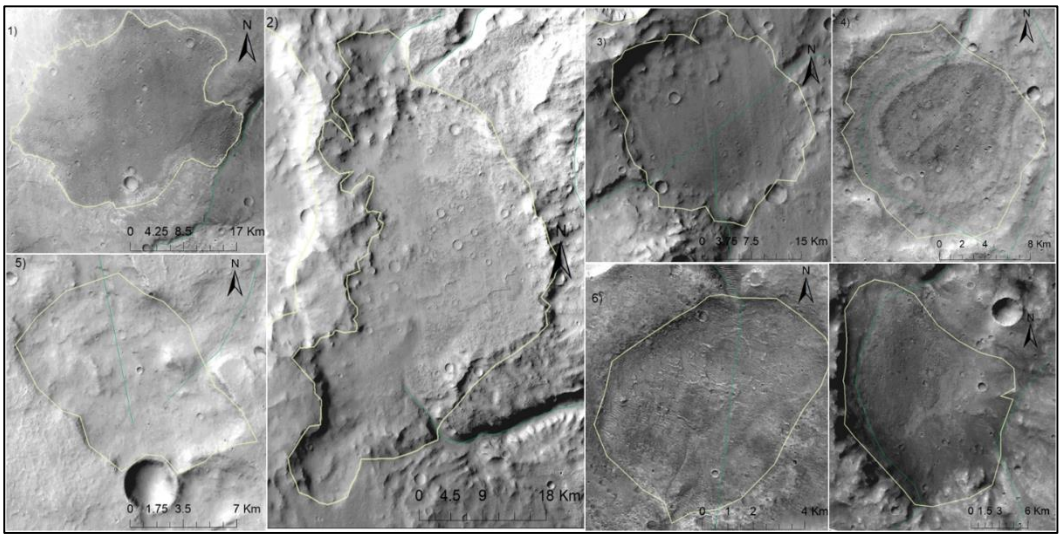


**Figure 5.7:** The determined open-basin lakes where the number of image for each lake corresponds the number in the lake name.

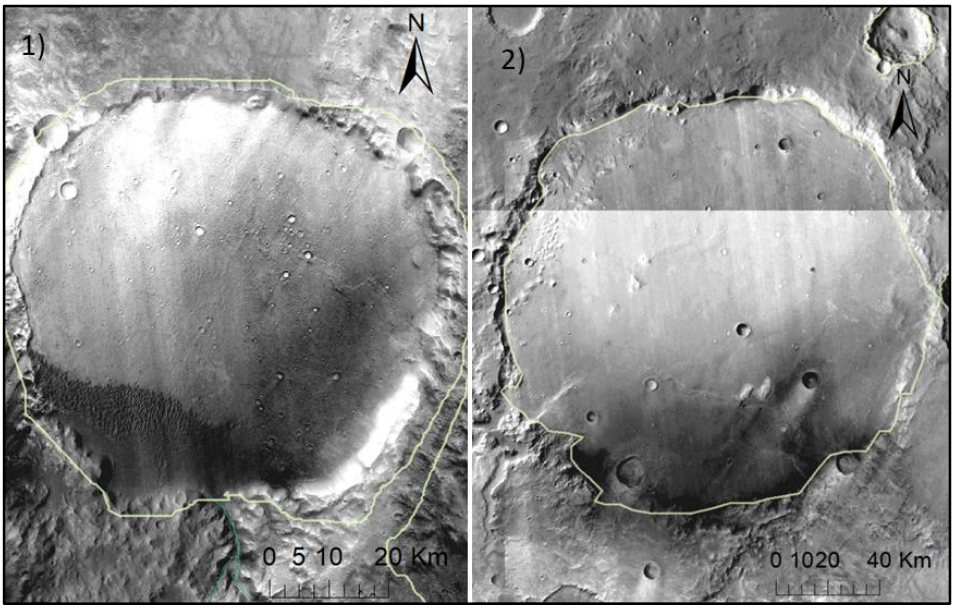


**Figure 5.8:** Two identified closed-basin lakes within area of interest.

To facilitate the analysis of the data, all measurements were projected onto the Mars_Equidistant_Cylindrical coordinate system, using the meter as the linear unit. The results of the analysis revealed that the lakes are distributed primarily along the valley network within the geographical boundaries of 131.9, -6.13 and 127.8, -10.81 Decimal degrees. Further details on the morphometric characteristics of the open-basin lakes, including their area, volume, and maximum depth, are presented in (Table 5.1). More detailed information about the minimum and maximum elevations and slopes are represented in the appendices Table 3. This dataset provides insights into the distribution and morphometry of paleolakes in the study area, and can be used to better understand the hydrological and geological history of Mars.

**Table 5.1:** Open-basin lakes data representing area, volume, elevation and slope, calculated using ArcMap and R studio

| Lake# | Area ($Km^2$) | Volume ($Km^3$) | Mean Elevation_0 (m)* | Mean Elevation (m)** | Mean Slope° |
|---|---|---|---|---|---|
| **O_1** | 210.94 | 11.27 | 53.44 | 380.44 | 0.49 |
| **O_2** | 366.06 | 80.39 | 219.62 | 1261.62 | 3.38 |
| **O_3** | 187.62 | 17.50 | 93.30 | 1101.30 | 2.49 |
| **O_4** | 65.25 | 2.20 | 33.66 | 1660.28 | 1.08 |
| **O_5** | 33.47 | 2.24 | 66.79 | 1635.79 | 2.17 |
| **O_6** | 15.23 | 0.50 | 32.87 | 1730.87 | 1.47 |
| **O_7** | 84.03 | 3.70 | 43.98 | 2087.98 | 1.58 |

*** Mean elevation referenced to 0 at the minimum elevation**
**** Mean elevation of actual elevation range without referencing**

The Open-basin lakes identified in the study exhibit irregular shapes and different sizes. The area of these lakes ranges from 15.2 $Km^2$ to 366.06 $Km^2$, with the largest lake being O_2 (Figure 5.9). The lowest mean elevation is found in O_1 at 380.4m, while the highest mean elevation is recorded in O_7 at 2087.98m (Figure 5.10). The volume of the open-basin lakes ranges from 0.50 $Km^3$ to 80.30 $Km^3$, with the largest volume recorded in O_2. Most of the open-basin lakes are connected to the main valley system, with some having an inlet and outlet. Specifically, Lakes O_1, O_3, O_6, and O_7 have an inlet, with the length of the inlet ranging from 1.5 Km for O_6 to 10.7 Km for O_3. The outlet of the open-basin lakes O_[2:7] is part of the main valley within the area and is believed to form a lake chain that extends for a length of 282.2 Km. This is displayed in Figure 1 in the appendices. The lake chain is divided into two groups; the first group contains four lakes located in the northern part of the valley, with a length of 20.1Km, while the other two lakes are located in the southern part of the basin.

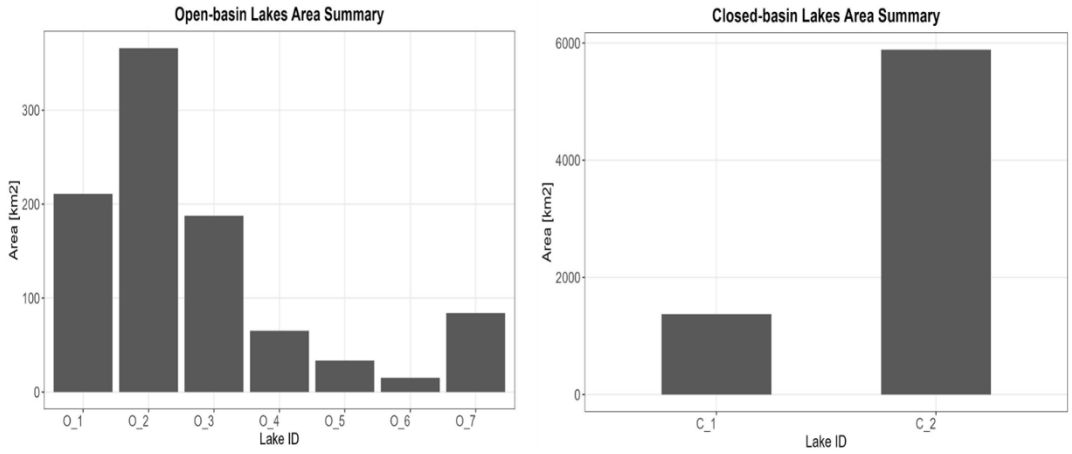


**Figure 5.9:** Area distribution of the open-basin lake and closed-basin lake

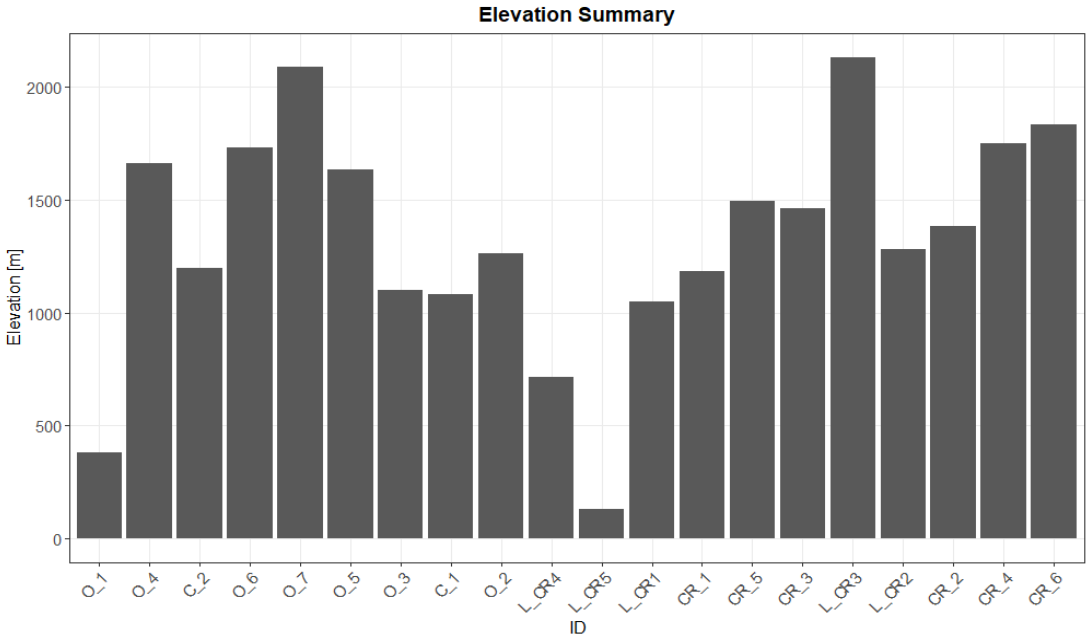


**Figure 5.10:** Summary of mean Elevations for the geomorphological landforms ordered from the lowest to the highest.

In the area of interest, two closed basin lakes have been identified, and their morphometric data has been summarized in (Table 5.2). Unlike the irregular shape of the open-basin lakes, these lakes have a more circular shape. The lakes are located in the southern part of the area of interest, and their XY coordinates can be found in Table 2 in the appendices section. These lakes have a large area of 1373.57 Km2 and 5885.98 Km2, with mean elevations above 1 km. The slopes of the lakes are relatively steep, with values of 3° and 1.29° for C_1 and C_2, respectively. Due to their large area and relatively high mean referenced elevations, the volume of the lakes is large, with values of 316.01$Km^3$ and 2953.94 $Km^3$ for C_1 and C_2, respectively. Both lakes have

inlets but no outlets. C_1 has two inlets with relatively long lengths of 40.4 and 16.3 Km, whereas C_2 has only one inlet with a length of 35.5 Km. The presence of inlets suggests that these lakes receive water from their surrounding watershed, which could potentially impact the water quality and characteristics of the lakes. The mean slope of the lakes varies from 0.43° in O_4 to 3.38° in O_2, with the majority of the lakes having slopes greater than 1° (Figure 5.11).

**Table 5.2:** Closed-basin lakes data representing area, volume, elevation and slope, calculated using ArcMap and R studio

| Lake# | Area (Km²) | Volume (Km³) | Mean Elevation_0 (m)* | Mean Elevation (m)** | Mean Slope° |
|---|---|---|---|---|---|
| **C_1** | 1373.57 | 316.01 | 230.06 | 1083.06 | 3.00 |
| **C_2** | 5885.98 | 2953.94 | 501.86 | 1197.86 | 1.29 |

*** Mean elevation referenced to 0 at the minimum elevation**
**** Mean elevation of actual elevation range without referencing**

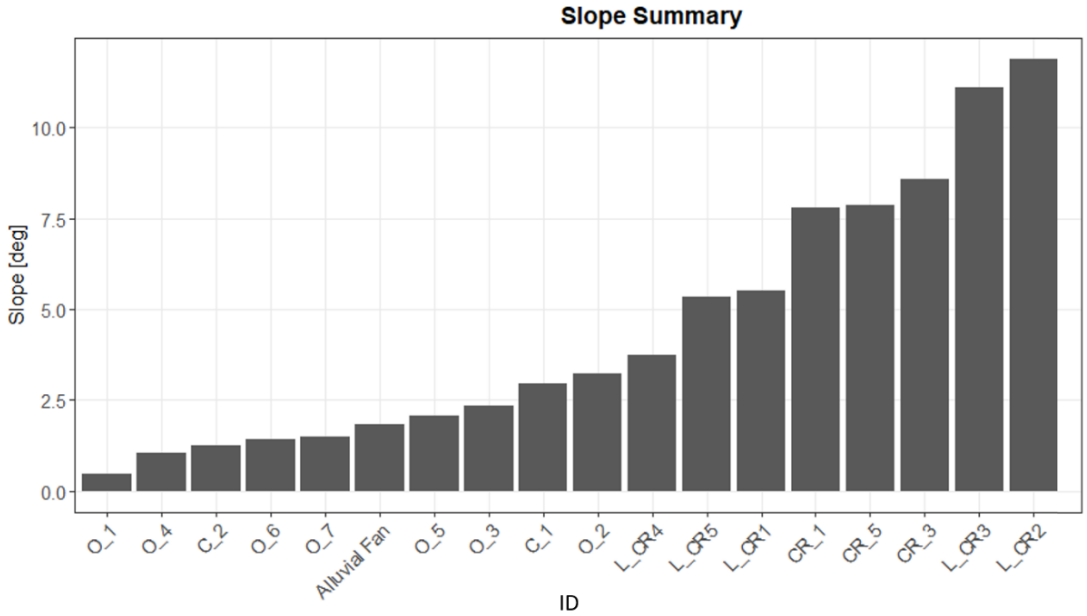


**Figure 5.11:** Summary of mean slopes for the geomorphological landforms ordered from the lowest to the highest.

## 5.4 Craters

An investigation of craters in the interested area was conducted using CTX mosaic image analysis. Six small craters were identified, with areas ranging from 1 to 6 $Km^2$. The mean elevation of the craters is between 1 to 2 Km, resulting in small volumes. CR_3 has the largest volume of 1.22 $Km^3$, while CR_2 has a very small volume

of 0.005 $Km^3$. Steep slopes were found in three of the craters, namely CR_1, CR_3, and CR_5, ranging from 7.4° to 9.6°, while the slope could not be calculated for the other three craters due to their small area, which is below 1.5 $Km^2$ (Figure 5.11). The maximum slope of the small craters ranges from 11.38° to 17.27°, while the minimum slope ranges from 3.43° to 4.7° (Table 4, in the appendices). These small craters were found near the valley networks, and some of them exhibit geological features, such as fan deposits covering the entire or part of the crater CR_4, CR_5 and CR_6 (Figure 5.12). CR_1, however, does not show any geomorphological features or changes on the surface. CR_5 and CR_6 are connected to the valley network. These craters are located in the middle to the south of the area within a range of 130.8, -7.5, and 129.9, -10.5 decimal degrees. The diameter of the small craters ranges from 1.13 to 2.6 Km, with CR_6 being the largest and CR_1 being the smallest (Table 5.3).

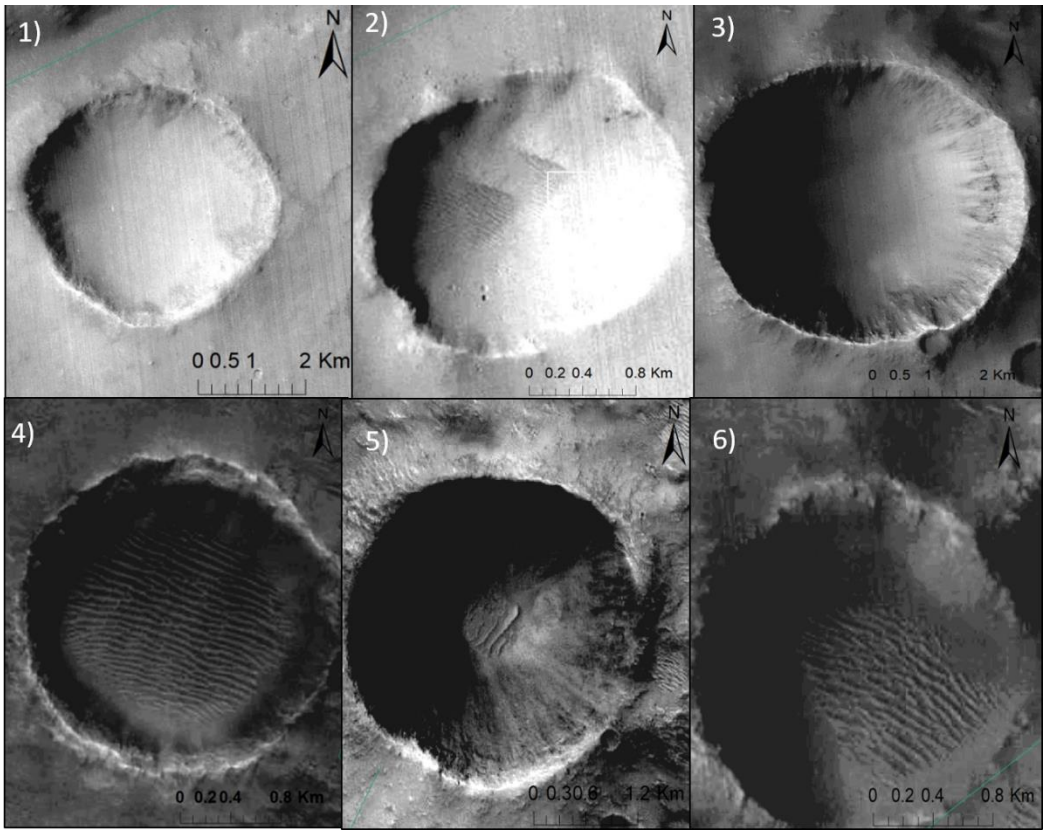


**Figure 5.12:** Six Detected small craters within the study area where the number in the figure reflects the number in their names.

During the exploration of the area, five large craters were also identified. These craters have a wider range of area, starting from 88.8 $Km^2$ in L_CR2 to 2827.7 $Km^2$ in L_CR4. Most of them have a mean elevation range from 1 to 2 Km, with L_CR5 being the only one with an elevation of 130.8m (Table 5.4). The range of volume for these craters is between 1705.39 to 29.38 $Km^3$. The mean slope ranges from 3.67° to 12°, showing high steepness. The largest crater in terms of area and volume has the

lowest mean elevation and slope. The maximum slope in all craters exceeds 20°, whereas the minimum slope is very small, below 0.2° (Table 5 in the appendices). These craters are distributed over the area of interest and have different geological features inside them.

**Table 5.3:** Small Crater data representing area, volume, elevation, slope and diameter, calculated using ArcMap and R studio

| Crater# | Area ($Km^2$) | Volume ($Km^3$) | Mean Elevation_0 (m)* | Mean Elevation (m)** | Mean Slope ° | Diameter (Km) |
|---|---|---|---|---|---|---|
| **CR_1** | 4.28 | 0.49 | 115.57 | 1184.57 | 7.43 | 2.60 |
| **CR_2** | 1.04 | 0.00 | 4.40 | 1383.40 | - | 1.50 |
| **CR_3** | 6.91 | 1.22 | 176.81 | 1460.81 | 9.02 | 2.90 |
| **CR_4** | 1.41 | 0.03 | 22.14 | 1751.14 | - | 1.35 |
| **CR_5** | 4.01 | 0.78 | 193.40 | 1495.40 | 9.56 | 1.80 |
| **CR_6** | 0.93 | 0.03 | 32.40 | 1831.40 | - | 1.13 |

*** Mean elevation referenced to 0 at the minimum elevation**
**** Mean elevation of actual elevation range without referencing**

**Table 5.4:** Large Crater data representing area, volume, elevation, slope and diameter, calculated using ArcMap and R studio

| Crater# | Area ($Km^2$) | Volume ($Km^3$) | Mean Elevation_0 (m)* | Mean Elevation (m)** | Mean Slope° | Diameter (Km) |
|---|---|---|---|---|---|---|
| **L_CR1** | 541.69 | 151.62 | 279.90 | 1047.90 | 5.77 | 25.25 |
| **L_CR2** | 88.79 | 38.55 | 434.15 | 1279.15 | 12.01 | 9.80 |
| **L_CR3** | 140.42 | 62.43 | 444.56 | 2130.56 | 11.11 | 13.40 |
| **L_CR4** | 2827.71 | 1705.39 | 603.10 | 713.21 | 3.67 | 55.00 |
| **L_CR5** | 112.24 | 29.38 | 261.80 | 130.80 | 5.52 | 10.20 |

*** Mean elevation referenced to 0 at the minimum elevation**
**** Mean elevation of actual elevation range without referencing**

L_CR2 and L_CR3 exhibit the presence of ridges over the surface of the crater, which can be observed in the (Figure 5.13). Additionally, a small mound can be seen on the surface of L_CR3. Fan deposits can be noticed in L_CR1 and L_CR5. Some of the craters are connected to the valley network, such as L_CR1, L_CR2, and L_CR3. L_CR4 is not connected to the valley, but it is adjacent to an open basin lake O_2, which has outlets to the valley. L_CR5 is quite far away from water sources. The diameter of the craters ranges from 10 Km to 55 Km, with L_CR4 having the largest diameter and L_CR2 having the smallest (Table 5.4).

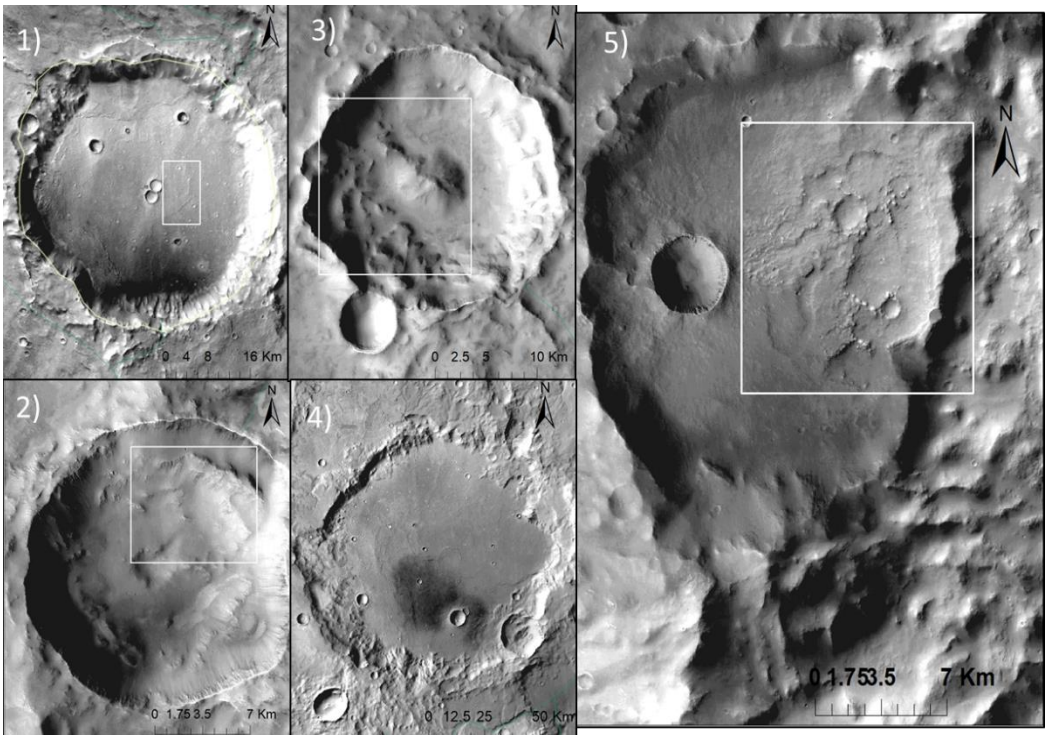


**Figure 5.13:** Five detected large craters within the study area where the number in the figure reflects the number in their names.

For the small crater they are identified to be smaller than 10 Km2 in area while the large crater are identified to be any larger Crater (Figure 5.14). The figure shows the difference in area between two craters. They are also differ in the shape and morphology where th small crater is more concise and the large craters are not very organzied in shape.

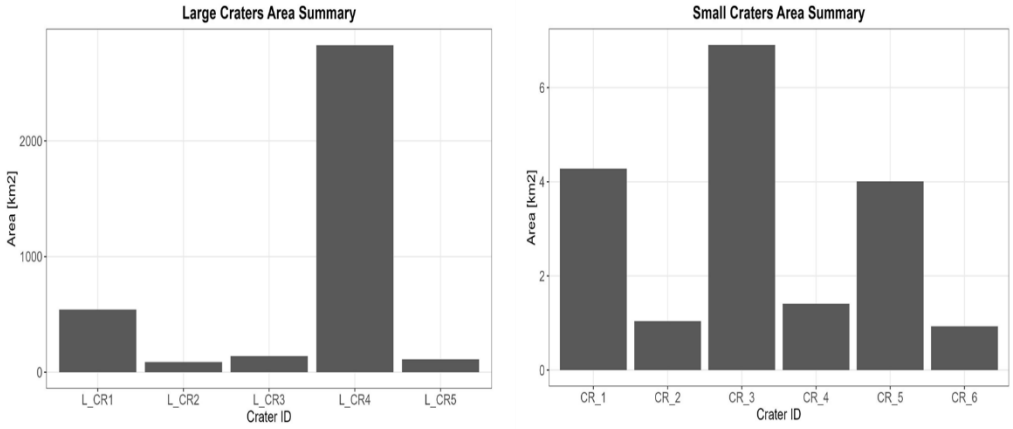


**Figure 5.14:** The area in Km2 to the large Craters and the small craters

## 5.5 Other Landforms

Apart from the prominent landforms, there are several other surface features on Mars that deserve attention. One such feature is a highland (L_1) located near the valley network and spanning a width of 650 m (as depicted in the figure 5.15). Another interesting set of formations are the small uplands that are clustered in two groups (L_2 and L_3) located approximately 6 Km away from the valley network. Group 1 (L_2) consists of seven small hills with a width ranging from 160 to 500 m, while Group 2 (L_3) is comprised of ten uplands with a smaller width range of 130 to 400 m. Most of these uplands have a conical shape and lack fractured structure.

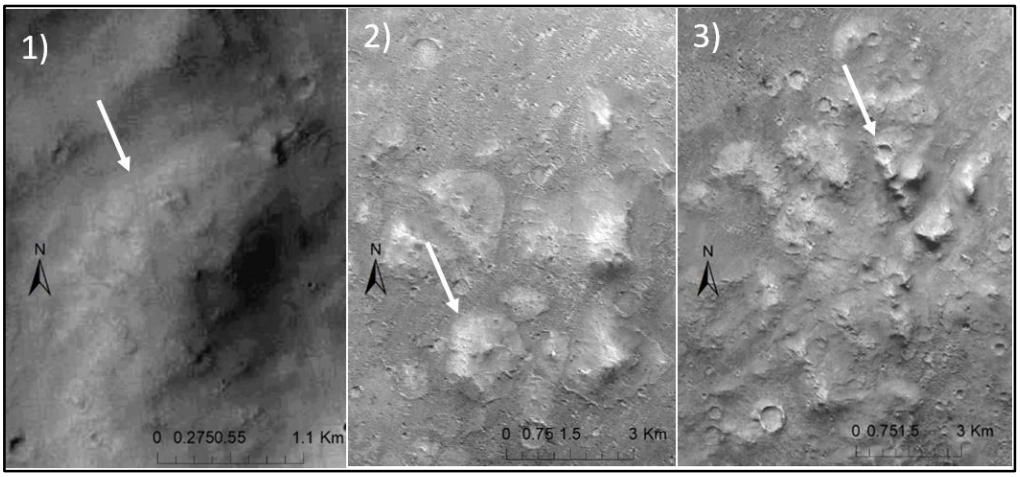


**Figure 5.15:** Various upland structures, 1) shows one upland, 2) and 3) shows group of small hill like structures

Furthermore, Mars exhibits other notable topographical features close in structure to flat-top highlands. Unlike the previously mentioned structures, these highlands are characterized by their flat tops and span a width range of 1.3 to over 5 kilometers. Through our analysis, we have identified three distinct flat-top highlands L_4, L_5 and L_6. They have irregular morphology and they are geographically separated mostly in the middle to a little south of the basin (Figure 5.16).

Another type of noteworthy surface feature on Mars is the collection of ridges known as ripple lands. These are identified as R_1, R_2, and R_3 in the study area, with R_1 and R_3 located near craters, while R_2 is situated between two open-basin lakes at a distance of roughly 8.2 Km from both lakes (Figure 5.17). While R_1 and R_3 are directly connected to the valley network, R_2 is situated at a distance of 1.5 Km from the potential flow of the valley channel. These structures are typically characterized by repeated ripple patterns and have a width range of 300 m to 1000 m, with lengths ranging from 6 km to 11 km. Additionally, there are several other ripple-shaped landforms identified in various locations, typically found within 1-3 Km

distance from the valley. These structures often exhibit single ripple patterns, as seen in R_4, R_5, and R_6, with lengths ranging from 2.5 to 8 Km and a width of 0.3 Km.

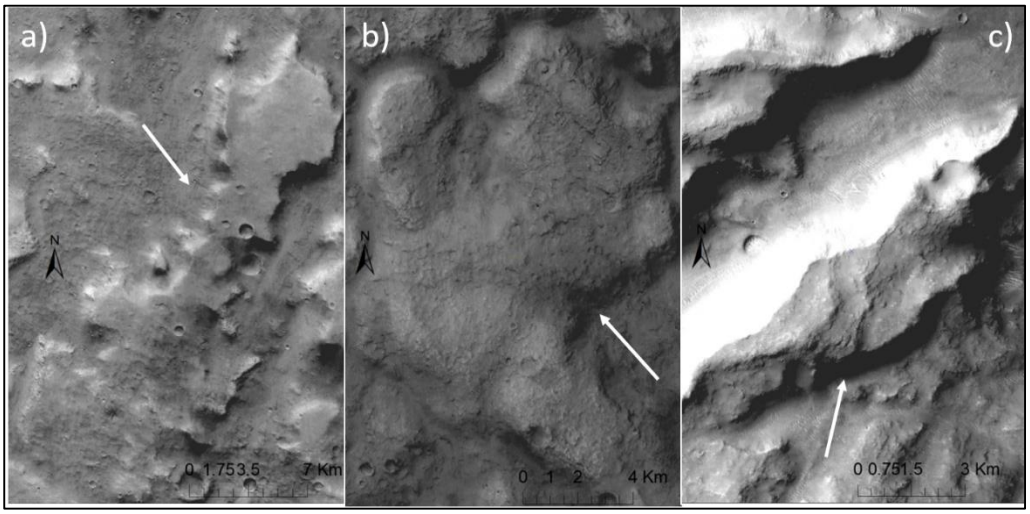


**Figure 5.16:** Top-flat highland within the valley basin. a) L_4, b) L5 and c) L_6

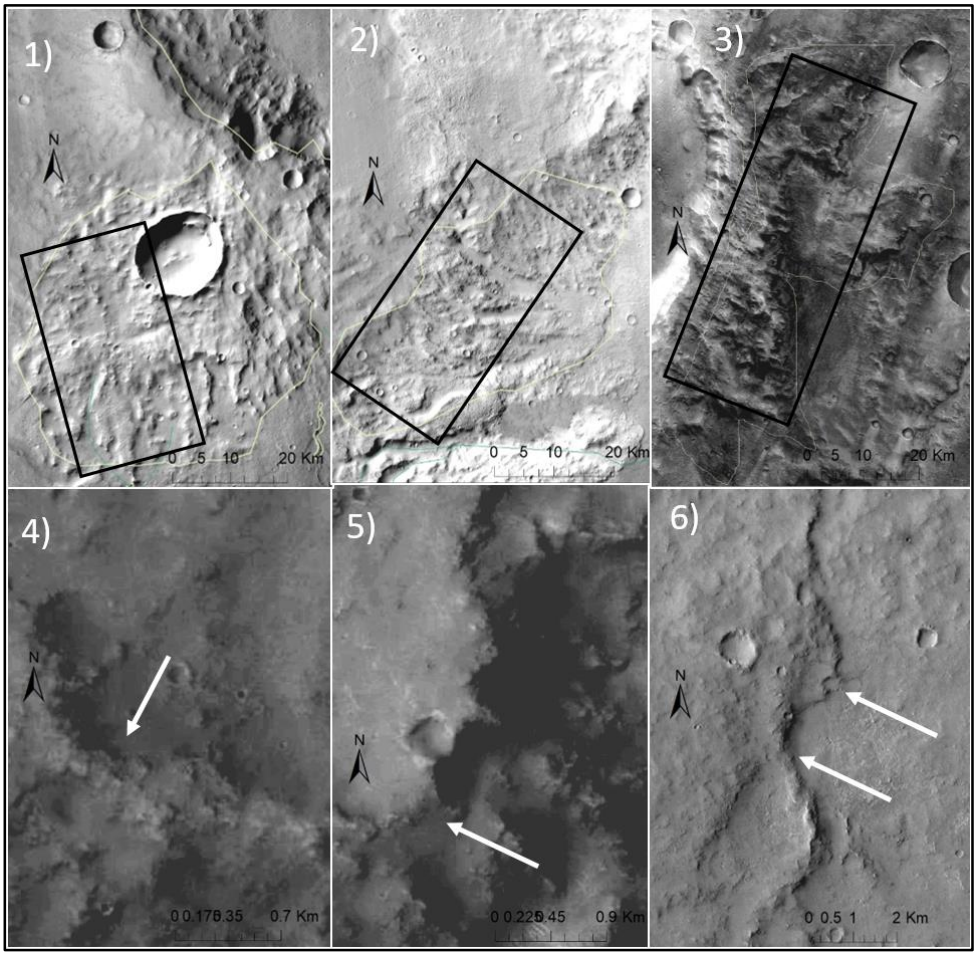


**Figure 5.17:** Ripple features found in repeated pattern (1, 2 and 3) and individual pattern (4,5 and 6).

One of the identified landforms (shown in the accompanying Figure 5.18) displays a distinct pattern of sediment deposition. The fan-shaped deposit (L_4) extends both horizontally and vertically, and it appears to have been formed by material moving in the different directions based on the aspect results of the area. This particular landform is located in close proximity to the valley network in the area, suggesting that it may have been influenced by the geological forces that shaped the network. Another notable landform in the area displays a polygonal pattern, with randomly arranged relief features (L_5). This landform is also located in close proximity to the valley network, and its formation may be related to the same geological processes that created the nearby fan-shaped deposit.

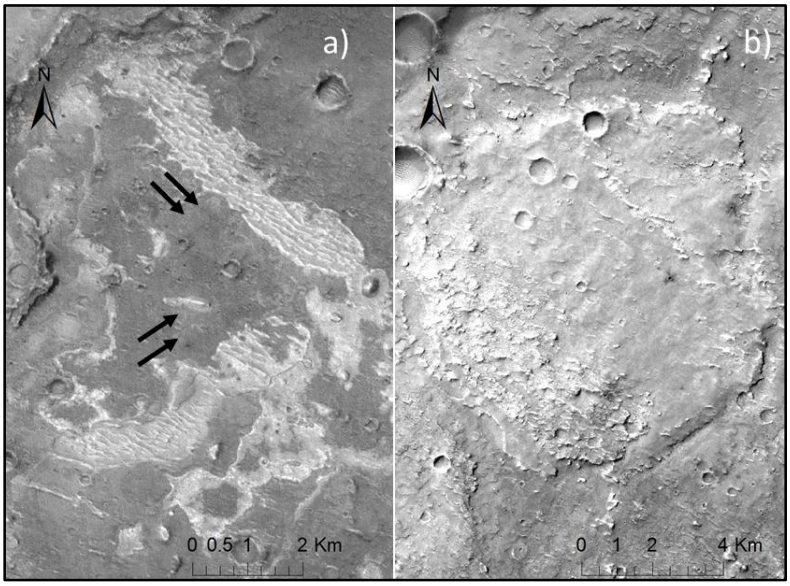


**Figure 5.18:** Two un-identified Patterns, a) shows fan layering structure and the black arrows represent the flow based on the aspect, b) shows polygonal relief features.

# 6 Discussion

The analysis of the area under investigation revealed a diverse range of geological landforms, including prominent features like paleolakes and impact craters located in various positions around the valley network. Moreover, structures resembling ridges and pingos were also identified. The area's unique location in the southern highlands of Mars, combined with its distinct composition of ridges, lakes, craters, and river channels, has led to a wide range of elevations observed in this region. This diverse topography may provide valuable insights into the geological and environmental conditions of this area.

## 6.1 Alluvial Fan

Based on the MOLA-DEM data, the alluvial fan on Mars appears to have characteristics similar to Sheet-flood fans found on Earth. Typically, Sheet-flood fans exhibit radial slopes that decrease from around 5° to 2°, while the detected fan on Mars shows a decrease from 7° to less than 1°. Sheet-flood fans are believed to form from sudden, unconfined water flow across a large area, often caused by heavy rainfall resulting in flash floods that rapidly expand onto nearby alluvial fans. The conical shape of an alluvial fan can promote the expansion of sheet-floods by allowing the water to spread out and cover a larger area. Sheet-floods can begin either at the top of the fan or on a depositional lobe downslope from an incised channel. One type of sheet-flood fan is the gravel poor sheet-flood fan, characterized by an average slope between 1.5° and 3°. This value is close to the average value for most of alluvial fans on Mars that range from 2° to 4° (Harish et al., 2021). The average slope of the fan understudy fills within this range suggesting that this fan could be constructed from poorly cemented sandstone bedrock, making them vulnerable to erosion. They typically exhibit minor rock-fall, rockslide, or rock-avalanche deposits and may have headward-eroding gullies, a desert pavement, and a coarse mantle. Disaggregation, rather than tectonic fracturing, may be the dominant process of bedrock erosion in this fan (Blair & Mcpherson, 2009).

Based on CTX stereo data, the alluvial fan on Mars appears to be primarily composed of clast-rich debris-flow lobes, with an average slope range of 3° to 8°. Debris flow is a sediment-gravity process generated by colluvial slope failures and may involve a mixture of sedimentary particles ranging in size from clay to gravel, along with entrained water and air. These flows move downslope in a viscous state under the force of gravity. The sediments in the fan could be coarser and more poorly sorted than the finer-grained sediment that can be formed on the upper portions of the fan, which may

make them more resistant to erosion and help to stabilize the fan over time. The edges of the lobes in these types of fans are sharply defined, with a fringe of coarse to very coarse pebbles and cobbles that are supported by the underlying sediment (Blair & Mcpherson, 2009). In addition, by comparing the fan characteristics with others from Mars, the fan is located close to the equator, which is similar to most of the discovered fans on Mars (Moore & Howard, 2005). It is also suggested that the sediment type in the fan may lay over the gravel type which is the sediment for most of the alluvial fans on Mars (Moore & Howard, 2005).

From the CTX mosaic, it appears that the fan is composed of two main lobes, with the one on the left extending up to 10 km and the one on the right extending up to 7-8 km away from the fan apex. The length between the traces extends from 300 m to 600 m. The disappearance of the cross-profile in the right section may be caused by several erosion factors, such as wind or the termination of the flow in this part. This is supported by the aspect results, which show that most of the flow goes in the north direction, which has a longer cross-fan profile shown downslope.

The difference between the CTX stereo and the MOLA-DEM datasets can be attributed to their varying resolutions. The CTX stereo boasts a higher resolution than the MOLA-DEM, which enables it to capture more intricate details that can significantly impact the slope and overall appearance of the fan. This increased level of detail afforded by the higher resolution allows for a deeper understanding of the fan's characteristics. As a result, the use of the CTX stereo dataset enables gaining a more precise understanding of the fan, as it is capable of capturing a greater number of pixels and finer details. The higher resolution of the CTX stereo dataset allows for a more comprehensive analysis of the fan, providing insights into its development and geological ancient history.

It is not only shown in the calculation of the slope but also can be seen in the calculation of volume. In addition, calculating the volume on pixel basis displayed difference by $1 * 10^{-4}$ when compared to the other method that is only accounts the absolute mean elevation of the fan.

The fan under study is classified as a medium scale fluvial fan with an area greater than 100 $Km^2$. Studies suggest that when the area exceeds 105 $Km^2$ and the radius is greater than 10 Km, it is considered to be a fluvial fan, which is a special type of alluvial fan (ZHANG et al., 2020). The origin of the sediment flow, whether it is mainly caused by gravity or by tractive currents, is also an important consideration. The sediment of a fluvial fan is typically transported by tractive currents, which are generated by the friction between the flowing water and the river bed (ZHANG et al., 2020). Tractive currents can move large particles such as boulders and cobbles and can also erode the river bed. This corresponds with the slopes calculated by the MOLA

DEM data, taking into consideration the area and the radius, it could be concluded that the higher possibility of the fan to be a fluvial fan.

On the other hand, alluvial fans are formed by the deposition of sediment carried by gravity flow and sheet flow. Gravity flow occurs when sediment is transported down the slope of the fan due to the force of gravity. Sheet flow occurs when water flows over a broad, shallow surface and transports sediment along with it (ZHANG et al., 2020). This is supported by the mean slope values resulting from the CTX stereo data. The difference in resolution between the CTX stereo and MOLA data highlights the importance of considering the level of detail required for a specific analysis. In this case, the higher resolution of the CTX data suggests that it may be more accurate and provide a more detailed understanding of the fan's characteristics. Based on the analysis of the CTX data, the fan is likely an alluvial fan, which is characterized by the deposition of sediment carried by water from upstream areas. This is supported by the nature of the sediments present in the fan, which are commonly found in alluvial fans.

When comparing the fan deposits on Mars with the structures of terrestrial fan formations, it is apparent that the Mars fan is most likely dominated by debris flow deposition (Figure 6.1). The layers of deposits found in the Martian fan are similar in morphology to those dominated by deposition according to (Harvey, A. M., 2012). A well-known example of a terrestrial alluvial fan is the fan in Death Valley, California (see Figure 6.2). Unlike the Martian fan, this terrestrial fan shows evidence of channel flow over the area, indicating that it has experienced much more erosion caused by water flow over time. While the martial indicated alluvial fan may be faced erosion events that erased the evidence of flow.

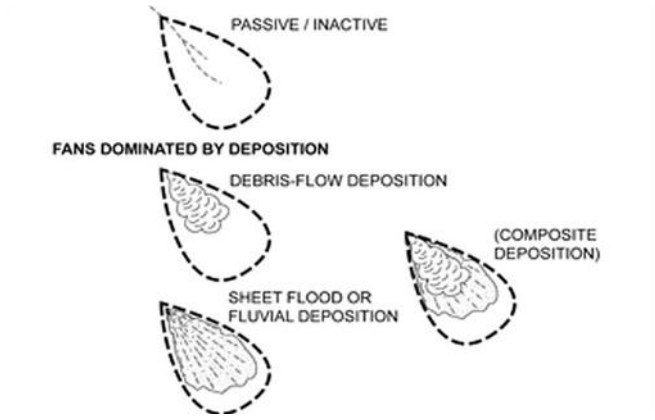


**Figure 6.1:** Terrestrial alluvial fans layer, Deposition state of fans, in terms of layers morphology (Harvey, A. M., 2012).

It is important to note that the classification of the fan as an alluvial fan is based on a combination of factors, including the nature of the sediments, the morphology of the fan, and the context of the surrounding landscape. Further analysis, including

additional data sources, may be necessary to confirm this classification and fully understand the processes that have shaped the fan over time.

**Figure 6.2:** Alluvial fan in the Death Valley, California,USA (Harvey, A. M., 2012).

## 6.2 Paleolakes

The area of interest contains both open-basin and closed-basin lakes, which are located within the previously suggested zone by other researchers, and are situated not lower than 30° (Caleb I. Fassett & James W. Head III, 2008). The open-basin lakes in this study have an area and volume that fall within the range of 210 lakes identified in the literature, which have a wide range of areas from 2 to 500,000 $Km^2$, and volumes from 0.02 to ~200,000 $Km^3$ (Caleb I. Fassett & James W. Head III, 2008). However, the open-basin lakes identified in this study have a smaller range than those reported in the literature, with the largest lake having an area of 367 $Km^2$ and a volume of 80 $Km^3$, both belonging to O_2. Despite being smaller in size, the area of the lakes can still be considered medium to small in comparison to Martian and terrestrial lakes.

Interestingly, there are some Earth lakes with similar areas to those identified in this study, such as Lake Ohrid in Southern Europe, which has an area of approximately 358$Km^2$ and a volume of 53.63$Km^3$, close to the area and volume of O_2. However, the lower volume of Lake Ohrid may be due to its shallower depth compared to O_2.

While the volume of the lakes can indicate the amount of water that can fill them, it may not necessarily provide an indication of the actual amount of water present in the area. Assuming that all the lakes were holding water at the same time, the total volume of water in this area would be 116.46 $Km^3$, representing the maximum amount of water that could fill the lakes at full capacity. This amount is equivalent to 8.04 * $10^{-4}$ GEL.

The presence of inlets and outlets is a key factor in the hydrology of lakes. However, in the case of three of the lakes in the study area, O_1, O_3, and O_4, no visible inlets are present. This suggests that these lakes may be fed by groundwater. However, it is important to note that previous studies have suggested that groundwater may play a larger role in feeding larger lakes (Clifford, 1993). This could be supported by the presence of knops on the surface of O_3 and O_5, which may indicate groundwater seepage. In contrast, knops are not present in O_1 and O_4.

In the case of O_6 and O_7, the inlet is fed from an adjacent crater and is part of the valley network within the study area. On the other hand, O_2 and O_5 are fed from attributes that originated from the main channel. The majority of the lakes in the study area are shallow due to the relatively steep slopes of the surrounding terrain.

The comparison between the open basin and closed basin lakes within the area of interest revealed a big difference in size. The open basin lakes had a much smaller area, all less than 500 $km^2$, while the closed basin lakes, C_1 and C_2, were larger, with areas of 1373.57 $km^2$ and 5885.98 $km^2$ respectively. This distinction in area resulted in the closed basin lakes having a much larger volume than their open basin counterparts, measuring approximately 316 $km^3$ and 2954 $km^3$ for C_1 and C_2 respectively. It is worth noting that Poyang Lake, China, has an area between the two closed basin lakes at 3210 $km^2$. However, its volume is significantly smaller at 25.2 $km^3$ due to its shallow depth of only 8.4m.

The volume of water required to fill both C_1 and C_2 lakes would be 3270 $km^3$, equivalent to 0.02 GEL. Their circular shape is typical of impact craters, as the lakes are often found within the craters. The large size of these closed basin lakes may be indicative of a complex hydrological system that involves both surface and subsurface water. The fact that they are closed basins, with no visible outlets, suggests that the water is being retained within the basin by some geological features such as faults or folds.

The characteristics of the inlets and slopes of the closed-basin lakes provide important insights into the hydrological dynamics of the region. The presence of inlets in these lakes indicates that the alluvial activity in the lake basin is predominantly supplied by valley networks around the lakes, rather than from groundwater. This is a key observation, as it suggests that the lakes are largely dependent on external water inputs, rather than on internal groundwater supply. In addition, the absence of outlets in these lakes implies that the water in the lakes is primarily reduced through evaporation. The long length of the inlets of C_1 and C_2 (with lengths greater than 20 Km) indicates that they fall into the category of long inlet valleys. These types of valleys are charac-

terized by a long and narrow shape. The gradual slope of the closed-basin lakes suggests that the lakes may be susceptible to erosion and sedimentation processes due to the fact that the slopes influence the velocity of water flowing into the lakes.

Understanding the sources of water for lakes is important for managing and conserving these valuable resources. Further investigation of the hydrological processes involved in the establishment and maintenance of these lakes may shed light on the complex interactions between surface water and groundwater in the study area.

## 6.3 Craters

The investigation of craters in the area under study revealed the presence of two distinct categories, small and large craters. The smooth surfaces of some of the small craters suggest that they may not have been involved in fluvial activity, or that the terraces created by water activity have been eroded by environmental factors. Interestingly, the formation of these craters does not appear to be the result of impacts, as their geomorphological structures differ. While the minimum slope of the small craters is higher than that of the larger craters, the maximum slope in the larger craters is higher. This may be due to the reliefs found on the edges of the larger craters allowing for gradual change of the slope in the crater edges, which are not present in the small craters and thus result in greater steepness. The small craters have regular circular shapes, with no irregularities, in contrast to impact craters. The fans observed on the surface may have been related the water activity as they are observed in CR_5 and CR_6 which are connected to the valley network.

It is interesting to note that the large craters in the area of interest have a depth that is relatively shallower than the previously detected craters such as Degana, Degana-A and Chukhung craters on Mars. They have 0.3 to 0.6 Km depth, while the detected craters have smaller depth between 0.7 to 2 Km. This could suggest that the area of interest has undergone different geological processes than the areas where the other craters were formed. As the Degana and Degana-A craters was suggested to be formed in Late Noachian era (Harish et al., 2021), while the craters in the area of interest suggested to be formed earlier in the middle Noachian period. In addition, the diameter of L_CR4 is closer to the Degana crater diameter, where L_CR4 is equal to 55 Km and Degana crater is 50 Km. Where L_CR1 has a close Diameter of 25.25 Km to the Degana-A that has a diameter equal to 20 Km. The Chukhung crater can be considered close to the area of L_CR4 as it is Diameter is 45 Km(Butcher et al., 2021). The similarity in shape to the Degana and Degana-A craters could indicate that they were formed by similar processes. The diameter of the large craters is also smaller compared to the adjacent Gale crater, which is one of the largest impact craters on Mars with diameter of 154 Km (Blake et al., 2013). However, it is important to note

that the size and depth of craters on Mars can vary greatly due to the different environmental conditions and geological processes that occur in different regions of the planet.

Moreover, the presence of these geological features in the large craters suggest that they have undergone different processes and events in the past compared to the small craters. The fans and ridges indicate the presence of water and fluvial activity, which could suggest that the area was once wetter and had more liquid water on the surface. The presence of alluvial activity in L_CR5 also suggests that water was present in the area, as alluvial fans are typically formed by the deposition of sediment by flowing water.

The large craters has more feature varities compared to the small craters such as fans and wrinkle ridges suggest that they maybe involved in fluvial activity in the past. The large craters in the study area exhibit a wide range of geological features, such as ridges and evidence of fluvial activity. L_CR1, for instance, displays ridges along its edges, which may be related to its connection with the valley network. The ridges present in L_CR2, L_CR3, and L_CR5 are similar to those found in the Chukhung crater. Interestingly, L_CR3 has a noticeable relief in its center, indicating the presence of a mound or pingo, which are mounds of ice that form in permafrost areas. This could suggest that the area was once colder and had a different climate than it does now. This feature is comparable to Mount Sharp, although on a smaller scale due to the difference in size between the two craters. L_CR3 also has a Lobate Debris Apron (LDA) that resembles the LDA found in Chukhung crater. inally, L_CR4 displays indications of fans over its surface, suggesting possible wind or erosion activities. Together, these features highlight the diversity of geological processes that have shaped the large craters in the study area.

Overall, the large craters in the area under study appear to have undergone a variety of geological processes and events, which can provide valuable insights into the geological history of the area and the planet as a whole.

## 6.4 **Other Landforms**

The identification of the uplands as pingos is supported by their width, which is in agreement with previous studies of pingos on Mars. These landforms are believed to have formed during a colder period in Mars' history when there was more water present. The location of these uplands between two potential valley delineations that are not visibly connected suggests the possibility of near to the surface water sources in the area. This water may have played a role in the formation of the two groups of pingos (L_2 and L_3). Additionally, the development of the single pingo shape (L_1)

may also be attributed to a subsurface water source. Understanding the potential presence of subterranean water on Mars is important for future exploration.

The flat-top highlands observed are significant geological structures that appear to have arisen due to fluvial activity that caused erosion to the surrounding area. 53 In our analysis, we have identified three such highlands that are located within the valley basin and are surrounded by at least two channels of the valley network. The irregular morphology of these highlands may have been caused by different water flow activity that led to the surface erosion around them leaving them with this structure. Another possibility that these structures were formed by the deposition of sediment over time, which then became resistant to erosion and ultimately formed the flat top. Alternatively, they could have been formed by the erosion of softer rock layers, leaving behind harder layers that resisted further erosion and formed the flat top.

The sinuous landforms in Degana-A crater have a ridge-like appearance (Harish et al., 2021), but the identified features are more densely clustered than those found in the Degana-A crater. They are located near a channel in the valley, suggesting that they were formed by the activity of flowing water. It is likely that the water eroded the surrounding area, resulting in the formation of these ridges. The presence of multiple features may be due to the flow of water from the crater in different directions. This could also explain why the other ridges have a single structure that does not directly intersect with the valley channels. Overall, these sinuous landforms offer valuable insights into the past fluvial activity of the area and help us understand the geological history of Mars.

The identification of these two landforms (L_4 and L_5) in the vicinity of the valley network could provide valuable insights into the geological processes that have shaped the Martian landscape. The sediment dispositioning pattern observed in the first landform suggests the action of a multidirectional flow, possibly associated with the transport and deposition of sediment by water. This finding could support the hypothesis of the presence of liquid water on Mars at some point in the past, and further investigations could reveal the timing and duration of these water-related processes.

# 7 Conclusion

The analysis of Mars satellite images near the equator has provided insights into the geological past of the planet. The discovery of a diverse range of landforms, each with their own unique characteristics, offers valuable clues to the geological processes that have shaped Mars over time. One of the most significant findings from this analysis is the presence of an alluvial fan with quite similar geomorphological characteristics to those found on Earth. This suggests that similar geological formation may have occurred on both planets, such as the deposition of sediment by flowing water. This offers an opportunity for comparative planetology, allowing us to gain a deeper understanding of the geologic processes that shape rocky planets like Earth and Mars.

Another significant finding from the analysis of the Mars satellite images is the identification of open-basin and closed-basin lakes. The presence of these lakes suggests that Mars has a complex hydrological system. The evidence gathered from these landforms indicates the possibility of flow of water on the planet in the past, especially during the Late-Noachian period. Furthermore, the amount of water that can fill the paleolakes has been estimated to be around 116.46 Km3, assuming the lakes were filled to their maximum at the same time. This provides valuable information about the amount of water that may have existed on Mars during this period, further adding to our understanding of the planet's past climate and hydrology.

Beside th lakes, the presence of about five impact craters, which show similarities in area to other craters on Mars. However, there are also significant differences in the depth of these craters, with some displaying ridges inside them. This indicates that the craters were formed through different geological processes and that the geological history of Mars is more complex than previously thought.

In addition to the impact craters, the wide variety of other landforms detected in the area also provide important clues about the planet's geographical history. The presence of different types of landforms, such as alluvial fans, pingos and lakes, suggests that the area has experienced significant changes in climate activity over time. This may have been influenced by a range of water sources, including groundwater, liquid water, and ice melting and flowing from high to low elevations.

The distinct differences in elevation and slopes between the various landforms detected in the area further suggest the diversity of geomorphological changes that have occurred over time. This highlights the importance of analyzing multiple landforms and their associated characteristics in order to gain a more comprehensive

understanding of the planet's geological history. By examining the unique features of each landform, we can piece together a more complete picture of the planet's past, including the processes that have shaped its surface and the environmental conditions that have prevailed throughout its history.

Further investigation is needed to fully understand the mechanisms that regulate the water balance of these closed basin lakes, as well as the formation and history of the craters in this region. Additional analysis of the watershed of the lakes and their contribution to the total watershed of the basin would provide more insights into the area's geology formation. It is also recommended to examine the knobs in the area with higher resolution data to ensure their presence, and to conduct soil analysis to better understand the composition and history of the landforms. Overall, continued investigation and analysis of the Mars landforms in the area of interest will provide important contributions to the field of planetary geology and our understanding of the Red Planet.

# 8 References


1. Adeli, S., Hauber, E., Kleinhans, M., Le Deit, L., Platz, T., Fawdon, P., & Jaumann, R. (2016). Amazonian-aged fluvial system and associated ice-related features in Terra Cimmeria, Mars. *Icarus*, *277*, 286–299. https://doi.org/10.1016/j.icarus.2016.05.020
2. Alemanno, G., Orofino, V., & Mancarella, F. (2018). Global Map of Martian Fluvial Systems: Age and Total Eroded Volume Estimations. Earth and Space Science, 5(10), 560–577. https://doi.org/10.1029/2018EA000362
3. Baker, V. R., Strom, R. G., Gulick, V. C., Kargel, J. S., G. Komatsu, & Kalet, V. S. (1991). Ancient oceans, ice sheets and the hydrological cycle on Mars. In *75. Centres for Disease Control Morbidity and Mortality Weekly Reports* (Vol. 4). Mahidol University Publication.
4. Berman, D. C., Chuang, F. C., Smith, I. B., & Crown, D. A. (2021). Ice-rich landforms of the southern mid-latitudes of Mars: A case study in Nereidum Montes. *Icarus*, *355*. https://doi.org/10.1016/j.icarus.2020.114170
5. Blair, T. C., & McPherson, J. G. (2009). Processes_and_Forms_of_Alluvial_Fans. *Springer*, 413–467.
6. Blake, D. F., Morris, R. V, Kocurek, G., Morrison, S. M., Downs, R. T., Bish, D., Ming, D. W., Edgett, K. S., Rubin, D., Goetz, † W, Madsen, M. B., Sullivan, R., Gellert, R., Campbell, I., Treiman, A. H., Mclennan, S. M., Yen, A. S., Grotzinger, J., Vaniman, D. T., … Sarrazin, P. (2013a). Curiosity at Gale Crater, Mars: Characterization and Analysis of the Rocknest Sand Shadow Downloaded from. In *www.sciencemag.org SCIENCE* (Vol. 341). http://science.sciencemag.org/
7. Burr, D. M., Soare, R. J., Wan Bun Tseung, J. M., & Emery, J. P. (2005). Young (late Amazonian), near-surface, ground ice features near the equator, Athabasca Valles, Mars. *Icarus*, *178*(1), 56–73. https://doi.org/10.1016/j.icarus.2005.04.012
8. Burr, D. M., Tanaka, K. L., & Yoshikawa, K. (2009). Pingos on Earth and Mars. *Planetary and Space Science*, *57*(5–6), 541–555. https://doi.org/10.1016/j.pss.2008.11.003
9. Butcher, F. E. G., Balme, M. R., Conway, S. J., Gallagher, C., Arnold, N. S., Storrar, R. D., Lewis, S. R., Hagermann, A., & Davis, J. M. (2021). Sinuous ridges in Chukhung crater, Tempe Terra, Mars: Implications for fluvial, glacial, and glaciofluvial activity. *Icarus*, *357*. https://doi.org/10.1016/j.icarus.2020.114131
10. Cabrol, N. A., & Grin, E. A. (1999). Distribution, Classification, and Ages of Martian Impact Crater Lakes. In *Icarus* (Vol. 142). http://www.idealibrary.comon
11. Cabrol, N. A., Grin, E. A., & Pollard, W. H. (2000). Possible Frost Mounds in an Ancient Martian Lake Bed. *Icarus*, *145*(1), 91–107. https://doi.org/10.1006/icar.1999.6326
12. Caleb I. Fassett, & James W. Head III. (2008). Valley network-fed, open-basin lakes on Mars: Distribution and implications for Noachian surface and subsurface hydrology. In *Icarus* (Vol. 198, Issue 1, pp. 37–56). American Geophysical Union. https://doi.org/10.1029/2004JE002287
13. Carr, M. H. (1996). *Water erosion on Mars and its biologic implications*.
14. Carr, M. H., & Head, J. W. (2010). Geologic history of Mars. *Earth and Planetary Science Letters*, *294*(3–4), 185–203. https://doi.org/10.1016/j.epsl.2009.06.042

15. Carr, M. H., & Head, J. W. (2015). Martian surface/near-surface water inventory: Sources, sinks, and changes with time. *Geophysical Research Letters*, *42*(3), 726–732. https://doi.org/10.1002/2014GL062464
16. Clifford, S. M. (1993). A model for the hydrologic and climatic behavior of water on Mars. *Journal of Geophysical Research*, *98*(E6). https://doi.org/10.1029/93je00225
17. Conway, S. J., & Balme, M. R. (2014). Decameter thick remnant glacial ice deposits on Mars. *Geophysical Research Letters*, *41*(15), 5402–5409. https://doi.org/10.1002/2014GL060314
18. Conway, S. J., Butcher, F. E. G., de Haas, T., Deijns, A. A. J., Grindrod, P. M., & Davis, J. M. (2018). Glacial and gully erosion on Mars: A terrestrial perspective. In *Geomorphology* (Vol. 318, pp. 26–57). Elsevier B.V. https://doi.org/10.1016/j.geomorph.2018.05.019
19. Dundas, C. M., & McEwen, A. S. (2010). An assessment of evidence for pingos on Mars using HiRISE. *Icarus*, *205*(1), 244–258. https://doi.org/10.1016/j.icarus.2009.02.020
20. Dundas, C. M., McEwen, A. S., Diniega, S., Byrne, S., & Martinez-Alonso, S. (2010). New and recent gully activity on Mars as seen by HiRISE. *Geophysical Research Letters*, *37*(7), n/a-n/a. https://doi.org/10.1029/2009gl041351
21. Dundas, C. M., Mellon, M. T., McEwen, A. S., Lefort, A., Keszthelyi, L. P., & Thomas, N. (2008). HiRISE observations of fractured mounds: Possible Martian pingos. *Geophysical Research Letters*, *35*(4). https://doi.org/10.1029/2007GL031798
22. Environmental Systems Research Institute (ESRI). (2012). ArcGIS Release 10.1. Redlands, CA.
23. Fassett, C. I., & Head, J. W. (2008). The timing of martian valley network activity: Constraints from buffered crater counting. *Icarus*, *195*(1), 61–89. https://doi.org/10.1016/j.icarus.2007.12.009
24. Fisher, D. A. (2005). A process to make massive ice in the martian regolith using long-term diffusion and thermal cracking. *Icarus*, *179*(2), 387–397. https://doi.org/10.1016/j.icarus.2005.07.024
25. Goudge, T. A., Aureli, K. L., Head, J. W., Fassett, C. I., & Mustard, J. F. (2015). Classification and analysis of candidate impact crater-hosted closed-basin lakes on Mars. *Icarus*, *260*, 346–367. https://doi.org/10.1016/j.icarus.2015.07.026
26. Greeley, R. (1987). Release of Juvenile Water on Mars: Estimated Amounts and Timing Associated with Volcanism. In *New Series* (Vol. 236, Issue 4809).
27. Grimm, R. E., & Painter, S. L. (2009). On the secular evolution of groundwater on Mars. *Geophysical Research Letters*, *36*(24). https://doi.org/10.1029/2009GL041018
28. Han, P. F., Wang, X. S., Wan, L., Jiang, X. W., & Hu, F. S. (2019). The exact groundwater divide on water table between two rivers: A fundamental model investigation. *Water (Switzerland)*, *11*(4). https://doi.org/10.3390/w11040685
29. Harish, Vijayan, S., & Mangold, N. (2021). Evidence for fluvial and glacial activities within impact craters that excavated into a Noachian volcanic dome on Mars. *Icarus*, *361*. https://doi.org/10.1016/j.icarus.2021.114397
30. Harvey, A. M., Mather, A. E., & Stokes, M. (2005). *Alluvial fans: geomorphology, sedimentology, dynamics-introduction. A review of alluvial-fan research*. https://www.lyellcollection.org
31. Harvey, A. M. (2012). The coupling status of alluvial fans and debris cones: a review and synthesis. Earth Surface Processes and Landforms, 37(1), 64-76.

32. Head, J. W., Mustard, J. F., Kreslavsky, M. A., Milliken, R. E., & Marchant, D. R. (2003). *Recent ice ages on Mars*. www.nature.com/nature
33. Hobley, D. E. J., Howard, A. D., & Moore, J. M. (2014). Fresh shallow valleys in the Martian midlatitudes as features formed by meltwater flow beneath ice. *Journal of Geophysical Research: Planets*, *119*(1), 128–153. https://doi.org/10.1002/2013JE004396
34. Hoke, M. R. T., Hynek, B. M., & Tucker, G. E. (2011). Formation timescales of large Martian valley networks. *Earth and Planetary Science Letters*, *312*(1–2), 1–12. https://doi.org/10.1016/j.epsl.2011.09.053
35. Holt, J. W., Safaeinili, A., Plaut, J. J., Head, J. W., Phillips, R. J., Seu, R., Kempf, S. D., Choudhary, P., Young, D. A., Putzig, N. E., Biccari, D., & Gim, Y. (2008). Radar sounding evidence for buried glaciers in the southern mid-latitudes of Mars. *Science*, *322*(5905), 1235–1238. https://doi.org/10.1126/science.1164246
36. Irwin, R. P., Howard, A. D., & Maxwell, T. A. (2004). Geomorphology of Ma'adim Vallis, Mars, and associated paleolake basins. In *Journal of Geophysical Research: Planets* (Vol. 109, Issue 12, pp. 1–33). American Geophysical Union. https://doi.org/10.1029/2004JE002287
37. Jouannic, G., Gargani, J., Costard, F., Ori, G. G., Marmo, C., Schmidt, F., & Lucas, A. (2012). Morphological and mechanical characterization of gullies in a periglacial environment: The case of the Russell crater dune (Mars). *Planetary and Space Science*, *71*(1), 38–54. https://doi.org/10.1016/j.pss.2012.07.005
38. Lammer, H., Selsis, F., Penz, T., V. Amerstorfer, U., Lichtenegger, H. I. M., Kolb, C., & Ribas, I. (2005). Atmospheric evolution and the history of water on mars. In *Advances in Astrobiology and Biogeophysics* (Vol. 4, pp. 25–43). Springer Verlag. https://doi.org/10.1007/978-3-540-31538-4_2
39. Malin, M. (2022). *CTX - NASA Mars*. MARS Reconnaissance Orbiter. https://www.msss.com/all_projects/mro-ctx.php
40. Malin, M. C., & Edgett, K. S. (2000). Evidence for recent groundwater seepage and surface runoff on Mars. *Science*, *288*(5475), 2330–2335. https://doi.org/10.1126/science.288.5475.2330
41. McEwen, A. (2022). *HiRISE - NASA Mars*. Lunar and Planetary Laboratory at the University of Arizona. https://mars.nasa.gov/mro/mission/instruments/hirise/
42. Michael, G. G. (2013). Planetary surface dating from crater size-frequency distribution measurements: Multiple resurfacing episodes and differential isochron fitting. *Icarus*, *226*(1), 885–890. https://doi.org/10.1016/j.icarus.2013.07.004
43. Moore, J. M., & Howard, A. D. (2005). Large alluvial fans on Mars. *Journal of Geophysical Research: Planets*, *110*(4), 1–24. https://doi.org/10.1029/2004JE002352
44. MarsSi. (2022). *MarsSI - Mars Data*. MARS Système d'Information. https://marssi.univ-lyon1.fr/wiki/Home
45. Orosei, R., Ding, C., Fa, W., Giannopoulos, A., Hérique, A., Kofman, W., Lauro, S. E., Li, C., Pettinelli, E., Su, Y., Xing, S., & Xu, Y. (2020a). The global search for liquid water on mars from orbit: Current and future perspectives. In *Life* (Vol. 10, Issue 8, pp. 1–15). MDPI AG. https://doi.org/10.3390/life10080120
46. Orosei, R., Ding, C., Fa, W., Giannopoulos, A., Hérique, A., Kofman, W., Lauro, S. E., Li, C., Pettinelli, E., Su, Y., Xing, S., & Xu, Y. (2020b). The global search for liquid water on mars from orbit: Current and future perspectives. In *Life* (Vol. 10, Issue 8, pp. 1–15). MDPI AG. https://doi.org/10.3390/life10080120

47. Orosei, R., Lauro, S. E., Pettinelli, E., Cicchetti, A., Coradini, M., Cosciotti, B., Di Paolo, F., Flamini, E., Mattei, E., Pajola, M., Soldovieri, F., Cartacci, M., Cassenti, F., Frigeri, A., Giuppi, S., Martufi, R., Masdea, A., Mitri, G., Nenna, C., … Seu, R. (2018). *Radar evidence of subglacial liquid water on Mars*.
48. Palucis, M. C., Dietrich, W. E., Williams, R. M. E., Hayes, A. G., Parker, T., Sumner, D. Y., Mangold, N., Lewis, K., & Newsom, H. (2016a\). Sequence and relative timing of large lakes in Gale crater (Mars) after the formation of Mount Sharp. *Journal of Geophysical Research: Planets*, *121*(3), 472–496. https://doi.org/10.1002/2015JE004905
49. Palumbo, A. M., Head, J. W., & Wordsworth, R. D. (2018). Late Noachian Icy Highlands climate model: Exploring the possibility of transient melting and fluvial/lacustrine activity through peak annual and seasonal temperatures. *Icarus*, *300*, 261–286. https://doi.org/10.1016/j.icarus.2017.09.007
50. Plaut, J. J., Picardi, G., Safaeinili, A., Ivanov, A. B., Milkovich, S. M., Cicchetti, A., Kofman, W., Mouginot, J., Farrell, W. M., Phillips, R. J., Clifford, S. M., Frigeri, A., Orosei, R., Federico, C., Williams, I. P., Gurnett, D. A., Nielsen, E., Hagfors, T., Heggy, E., … Edenhofer, P. (2007). Subsurface radar sounding of the south polar layered deposits of Mars. *Science*, *316*(5821), 92–95. https://doi.org/10.1126/science.1139672
51. Richardson, M. I., & Mischna, M. A. (2005). Long-term evolution of transient liquid water on Mars. *Journal of Geophysical Research: Planets*, *110*(3), 1–21. https://doi.org/10.1029/2004JE002367
52. Rosenberg, E. N., & Head, J. W. (2015). Late Noachian fluvial erosion on Mars: Cumulative water volumes required to carve the valley networks and grain size of bed-sediment. *Planetary and Space Science*, *117*, 429–435. https://doi.org/10.1016/j.pss.2015.08.015
53. Rosenberg, E. N., Palumbo, A. M., Cassanelli, J. P., Head, J. W., & Weiss, D. K. (2019). The volume of water required to carve the martian valley networks: Improved constraints using updated methods. *Icarus*, *317*, 379–387. https://doi.org/10.1016/j.icarus.2018.07.017
54. RStudio Team (2020). RStudio: Integrated Development for R. RStudio, PBC, Boston, MA URL http://www.rstudio.com/
55. Schon, S. C., Head, J. W., & Fassett, C. I. (2012). Recent high-latitude resurfacing by a climate-related latitude-dependent mantle: Constraining age of emplacement from counts of small craters. *Planetary and Space Science*, *69*(1), 49–61. https://doi.org/10.1016/j.pss.2012.03.015
56. Tanaka, K. L., Skinner, J. A., Dohm, J. M., Irwin, R. P., Kolb, E. J., Fortezzo, C. M., Platz, T., Michael, G. G., & Hare, T. M. (2014a). *Geologic Map of Mars*.
57. Tanaka, K. L., Skinner, J. A., Dohm, J. M., Irwin, R. P., Kolb, E. J., Fortezzo, C. M., Platz, T., Michael, G. G., & Hare, T. M. (2014b). *USGS Scientific Investigations Map 3292, mapsheet*. https://doi.org/10.3133/sim3292
58. Villanueva, G. L., Mumma, M. J., Novak, R. E., Käufl, H. U., Hartogh, P., Encrenaz, T., Tokunaga, A., Khayat, A., & Smith, M. D. (2017). *Strong water isotopic anomalies in the martian atmosphere: Probing current and ancient reservoirs Downloaded from*. http://science.sciencemag.org/
59. Williams, R. M. E., Irwin, R. P., Burr, D. M., Harrison, T., & McClelland, P. (2013). Variability in martian sinuous ridge form: Case study of aeolis serpens in the aeolis dorsa, mars, and insight from the mirackina paleoriver, South Australia. *Icarus*, *225*(1), 308–324. https://doi.org/10.1016/j.icarus.2013.03.016

60. Williams, R. M. E., & Phillips, R. J. (2001). Morphometric measurements of martian valley networks from Mars Orbiter Laser Altimeter (MOLA) data. *Journal of Geophysical Research: Planets*, *106*(E10), 23737–23751. https://doi.org/10.1029/2000JE001409
61. Winter, T. C., Rosenberry, D. O., & Labaugh, J. W. (2003). Where Does the Ground Water in Small Watersheds Come From? *GroundWater*, *41*(7), 989–1000. https://doi.org/10.1111/j.1745-6584.2003.tb02440.x
62. Xiao, L., Huang, J., Christensen, P. R., Greeley, R., Williams, D. A., Zhao, J., & He, Q. (2012). Ancient volcanism and its implication for thermal evolution of Mars. *Earth and Planetary Science Letters*, *323–324*, 9–18. https://doi.org/10.1016/j.epsl.2012.01.027
63. Yung, Y. L., Wen, J.-S., Pinto, J. P., Allen, M., Pierce, K. K., & Paulson, S. (1988). HDO in the Martian Atmosphere: Implications for the Abundance of Crustal Water 1. In *ICARUS* (Vol. 76).
64. ZHANG, Y., DAI, X., WANG, M., & LI, X. (2020). The concept, characteristics and significance of fluvial fans. *Petroleum Exploration and Development*, *47*(5), 1014–1026. https://doi.org/10.1016/S1876-3804(20)60113-6

# List of Abbreviations

| | |
|---|---|
| **GEL** | Global Equivalent Layer |
| **PLD** | Polar Layered Deposits |
| **LDM** | Latitude-Dependent Mantle |
| **LDA** | Lobate Debris Aprons |
| **LVF** | Lineated Valley Fill |
| **CCF** | Concentric Crater Fill CCF |
| **MOLA** | Mars Orbiter Laser Altimeter |
| **HDO** | Heavy Water |
| **IGF** | Inter-Basin Groundwater Flow |
| **mNh** | Middle Noachian Highland |
| **eNh** | Early Noachian Highland Unit |
| **HNtu** | Hesperian And Noachian Transition Unit |
| **MSL** | Mars Science Laboratory–Curiosity |
| **MRO** | Mars Reconnaissance Orbiter |
| **CTX** | Context Camera |
| **HiRISE** | High-Resolution Imaging Science Experiment |
| **CRISM** | The Compact Reconnaissance Imaging Spectrometer For Mars |
| **MGS** | Mars Global Surveyor Mission |

# List of Figure

# List of Tables

# Appendices

**Closed/ Open-basin Lake chain**

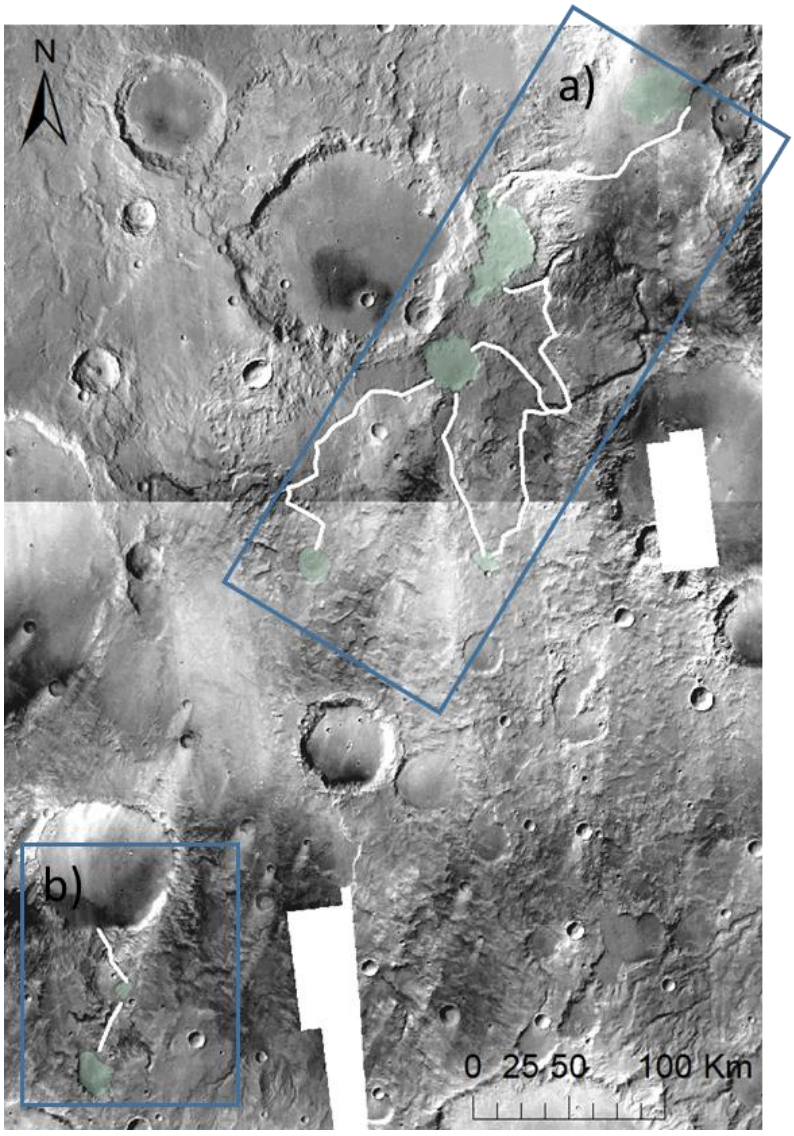


**Figure 0.1:** The chains that connect Open-basin lake, a) the first chain with length 282.2 Km, b) the second chain with length of 20.1 Km, the chains drawn by the guide from the martial valley system database (Alemanno, 2018).

**Table 1:** Satellite Data sources.

| Data | Sources |
|---|---|
| **CTX Mosaic** | https://www.arcgis.com/home/search.html?q=owner%3Aesri_astro |
| **CTX stereo** | https://marssi.univ-lyon1.fr/MarsSI/ |
| **HiRISE** | https://marssi.univ-lyon1.fr/MarsSI/ |
| **MOLA** | https://astrogeology.usgs.gov/search/map/Mars/GlobalSurveyor/MOLA |

**Table 2:** The XY coordinates for identified lakes and craters

| Crater# | X coordinate | Y coordinate | Lake# | X coordinate | Y coordinate |
|---|---|---|---|---|---|
| **CR_1** | -2914523 | -445428.9 | **O_1** | -2845984 | -361482 |
| **CR_2** | -2927721 | -448019.7 | **O_2** | -2889302 | -403591 |
| **CR_3** | -2988118 | -470130.2 | **O_3** | -2902599 | -435425 |
| **CR_4** | -2953488 | -615797 | **O_4** | -2940755 | -491452 |
| **CR_5** | -2942462 | -568798.6 | **O_5** | -2893113 | -490445 |
| **CR_6** | -2960583 | -627746.6 | **O_6** | -2993396 | -609224 |
| **L_CR1** | -2931433 | -541702.2 | **O_7** | -3001411 | -633056 |
| **L_CR2** | -2987408 | -490502.2 | **C_1** | -2997920 | -575194 |
| **L_CR3** | -3001096 | -438477.9 | **C_2** | -3039373 | -493025 |
| **L_CR5** | -2929809 | -403919.5 | | | |
| **L_CR4** | -2824924 | -368011.3 | | | |

**Table 3:** The Minimum and Maximum slope and elevation for the determined lakes

| Lake# | Min Elevation (m) | Max Elevation (m) | Min Slope° | Max Slope° |
|---|---|---|---|---|
| **O_1** | 327.00 | 447.00 | 0.02 | 2.71 |
| **O_2** | 1042.00 | 2063.00 | 0.02 | 19.08 |
| **O_3** | 1008.00 | 1751.00 | 0.03 | 17.86 |
| **O_4** | 1626.61 | 1767.12 | 0.03 | 1.50 |
| **O_5** | 1569.00 | 1786.00 | 0.35 | 5.62 |
| **O_6** | 1698.00 | 1778.00 | 0.48 | 2.79 |
| **O_7** | 2044.00 | 2289.00 | 0.11 | 9.82 |
| **C_1** | 853.00 | 2279.00 | 0.00 | 31.58 |
| **C_2** | 696.00 | 2023.00 | 0.00 | 21.72 |

**Table 4:** The Minimum and Maximum slope and elevation for the determined small craters

| Crater# | Min Elevation (m) | Max Elevation (m) | Min Slope° | Max Slope° |
|---|---|---|---|---|
| **CR_1** | 1069.00 | 1287.00 | 4.68 | 11.38 |
| **CR_2** | 1379.00 | 1389.00 | - | - |
| **CR_3** | 1284.00 | 1591.00 | 3.71 | 14.29 |
| **CR_4** | 1729.00 | 1773.00 | - | - |
| **CR_5** | 1302.00 | 1611.00 | 3.43 | 17.27 |
| **CR_6** | 1799.00 | 1870.00 | - | - |

**Table 5:** The Minimum and Maximum slope and elevation for the determined small craters

| Crater# | Min Elevation (m) | Max Elevation (m) | Min Slope° | Max Slope° |
|---|---|---|---|---|
| **L_CR1** | 768.00 | 2029.00 | 0.02 | 25.94 |
| **L_CR2** | 845.00 | 1885.00 | 0.07 | 23.72 |
| **L_CR3** | 1686.00 | 2810.00 | 0.19 | 25.42 |
| **L_CR4** | 110.11 | 2533.40 | 0.01 | 29.95 |
| **L_CR5** | -131.00 | 764.00 | 0.02 | 20.27 |